



Implementing a dynamic representation of fire and harvest including subgrid-scale heterogeneity in the tile-based land surface model CLASSIC v1.45

Salvatore R. Curasi^{1,2}, Joe R. Melton¹, Elyn R. Humphreys², Txomin Hermosilla³, and Michael A. Wulder³

¹Climate Research Division, Environment, and Climate Change Canada, Victoria, BC, V8N 1V8, Canada

²Department of Geography & Environmental Studies, Carleton University, Ottawa, ON, K1S 5B6, Canada

³Canadian Forest Service (Pacific Forestry Centre), Natural Resources Canada, Victoria, BC, V8Z 1M5, Canada

Correspondence: Salvatore R. Curasi (sal.curasi@ec.gc.ca)

Received: 31 August 2023 – Discussion started: 8 September 2023

Revised: 14 February 2024 – Accepted: 28 February 2024 – Published: 12 April 2024

Abstract. Canada's forests play a critical role in the global carbon (C) cycle and are responding to unprecedented climate change as well as ongoing natural and anthropogenic disturbances. However, the representation of disturbance in boreal regions is limited in pre-existing land surface models (LSMs). Moreover, many LSMs do not explicitly represent subgrid-scale heterogeneity resulting from disturbance. To address these limitations, we implement harvest and wild-fire forcings in the Canadian Land Surface Scheme Including Biogeochemical Cycles (CLASSIC) land surface model alongside dynamic tiling that represents subgrid-scale heterogeneity due to disturbance. The disturbances are captured using 30 m spatial resolution satellite data (Landsat) on an annual basis for 33 years. Using the pan-Canadian domain (i.e., all of Canada south of 76° N) as our study area for demonstration, we determine the model setup that optimally balances a detailed process representation and computational efficiency. We then demonstrate the impacts of subgrid-scale heterogeneity relative to standard average individual-based representations of disturbance and explore the resultant differences between the simulations. Our results indicate that the modeling approach implemented can balance model complexity and computational cost to represent the impacts of subgrid-scale heterogeneity resulting from disturbance. Subgrid-scale heterogeneity is shown to have impacts 1.5 to 4 times the impact of disturbance alone on gross primary productivity, autotrophic respiration, and surface energy balance processes in our simulations. These impacts are a result of subgrid-scale heterogeneity slowing vegetation regrowth and affecting surface energy balance in recently dis-

turbed, sparsely vegetated, and often snow-covered fractions of the land surface. Representing subgrid-scale heterogeneity is key to more accurately representing timber harvest, which preferentially impacts larger trees on higher quality and more accessible sites. Our results show how different discretization schemes can impact model biases resulting from the representation of disturbance. These insights, along with our implementation of dynamic tiling, may apply to other tile-based LSMs. Ultimately, our results enhance our understanding of, and ability to represent, disturbance within Canada, facilitating a comprehensive process-based assessment of Canada's terrestrial C cycle.

Copyright statement. © His Majesty the King in Right of Canada, as represented by the Minister of Environment and Climate Change, 2024.

1 Introduction

Canada's forests play a critical role in the global carbon (C) cycle (Keenan and Williams, 2018; Lenton et al., 2008). Canada's forests are also responding to both unprecedented climate change and ongoing anthropogenic disturbance (Lenton et al., 2008; White et al., 2017). Unfortunately, disentangling the relative impacts of disturbance processes and climate change on the Canadian forest C cycle is difficult (Sulla-Menashe et al., 2018; Goetz et al., 2005; Ju and Masek, 2016; Weber and Flannigan, 1997). Process-based land surface models (LSMs) provide a tool to evalu-

ate the impacts of both types of disturbance, but there has only been limited representation of anthropogenic disturbance in regional or global C cycling assessments (Friedlingstein et al., 2019; Peng et al., 2014; Chaste et al., 2017; Hayes et al., 2012). Moreover, of those LSMs that do explicitly represent anthropogenic disturbance, only a small subset account for the resulting subgrid-scale heterogeneity (Le Quéré et al., 2018; Nabel et al., 2020; Pongratz et al., 2018). Here we demonstrate the impacts of disturbance and subgrid-scale heterogeneity on C and energy fluxes by implementing a dynamic tiling scheme in the Canadian Land Surface Scheme Including Biogeochemical Cycles (CLASSIC).

Subgrid-scale landscape heterogeneity refers to any characteristic of the landscape that differs at scales below that of the main model grid – in this case, differences in tree age and biomass in the burned or harvested subfraction of the grid cell. Tile-based LSMs, unlike individual-based models (i.e., models which simulate the landscape using several heterogeneous individuals), do not inherently represent subgrid-scale heterogeneity. Instead, the tile represents the average individual of a given plant function type (PFT) and thus represents the PFT's average state within the grid cell (a single height, biomass, etc.), which is used to simulate fluxes. Although most tile-based LSMs account for wood harvest, few represent the resulting subgrid-scale landscape heterogeneity, instead representing the impact of disturbances on the average individual PFT (Le Quéré et al., 2018; Pongratz et al., 2018; Nabel et al., 2020).

Stand-replacing forest disturbances (i.e., timber harvest and fire) directly impact forest C stocks through the removal of standing biomass (Wulder et al., 2020). In addition, stand-replacing disturbances also impact stand structure, especially in the case of managed timber harvest (Pan et al., 2010; Kuvuvainen and Gauthier, 2018; Pan et al., 2013). The resulting stand structure impacts forest function such as the exchange of matter and energy with the atmosphere as well as the forest's response to climate change (Erb et al., 2017; Luysaert et al., 2014; Körner, 2006; Dore et al., 2010; Liu, 2005; Maness et al., 2012; Hirano et al., 2017). Historically, 0.4 % of Canada's ~ 650 Mh of forested ecosystems are affected by stand-replacing disturbance per year (White et al., 2017). The age structure of Canadian forests due to historical disturbance has impacted the strength of the historical C sink in Canadian forests (Kurz and Apps, 1999, 1993; Böttcher et al., 2008). The age structure resulting from disturbance also influences the surface energy balance of stands by, for example, altering the sensible heat flux due to differences in snow cover and albedo and altering the seasonality of surface energy budgets and land surface properties (Liu, 2005; Maness et al., 2012). Therefore, it is key that we enhance our ability to accurately represent both disturbance processes and the influence of the subgrid-scale heterogeneity that disturbances produce within LSMs.

Disturbance events impact the response of Canada's forests to climate change. The responses of forest produc-

tivity, forest soil decomposition processes, and evaporation rates to warming, rising CO₂ concentrations, and changes to precipitation regimes will depend on stand structural characteristics and tree species characteristics (Hember et al., 2012; Kurz et al., 1997; Körner, 2006; Shrestha and Chen, 2010; Bond-Lamberty and Gower, 2008; Czimczik et al., 2006; Kurz et al., 2008). Warmer temperatures and higher atmospheric CO₂ concentrations are likely to increase the productivity of boreal forests, whereas drought stress and changing disturbance regimes are likely to decrease productivity and enhance the decomposition of soil C, leading to a patchwork of contrasting future responses (Babst et al., 2019; Reich et al., 2018; Lenton et al., 2008; Weber and Flannigan, 1997; Potapov et al., 2008; Ju and Chen, 2008; Sulla-Menashe et al., 2018). Complex changes in vegetation productivity have already been observed across the pan-Canadian domain due to the intermingling of different disturbance regimes and different vegetation sensitivities to climate change (Marchand et al., 2018; D'Orangeville et al., 2018; Ma et al., 2012; Girardin et al., 2016). Decreases in vegetation productivity are generally occurring in north-western boreal forests, whereas southeastern boreal forests show positive trends (Marchand et al., 2018). Much of the landscape-scale change in vegetation productivity detected across Canada's boreal forests is a product of or is influenced by stand-replacing disturbance (Hermosilla et al., 2015b, a). Some negative productivity trends in the southern fringes of western undisturbed forests can be largely be attributed to moisture stress, and some of the positive trends in cooler and wetter portions of eastern boreal forests can be attributed to warming (Marchand et al., 2018; Sulla-Menashe et al., 2018). Process-based models which represent both disturbance and the resultant subgrid-scale landscape heterogeneity can offer insight into the drivers of these complex trends (Böttcher et al., 2008).

CLASSIC is a tile-based LSM that can be coupled to the Canadian Earth System Model (CanESM). Several methods are available for representing disturbance history in tile-based LSMs. Some models represent the age classes within the stand by using a fixed number of tiles to represent fractional areas below the scale of the main model grid (i.e., from two to 12 tiles) (Shevliakova et al., 2009; Yue et al., 2018a; Naudts et al., 2015; Yang et al., 2010; Stocker et al., 2014). Alternatively, several models simulate subgrid-scale forest structure using another model housed in a separate module coupled to the main model (Bellassen et al., 2010; Haverd et al., 2014). The module takes information about net primary productivity from the main model and uses it to simulate and track the growth of individual trees. The module then returns grid-cell average state information (i.e., biomass and litter fluxes), which is used by the main model to simulate subsequent fluxes. Finally, a recently developed approach uses a fixed number of tiles to represent age classes (Nabel et al., 2020). Tile fractional area and associated state variables (i.e., biomass C) are horizontally exchanged between

the tiles to represent processes like aging, harvest, and disturbance. Each approach entails a host of strengths and weaknesses as well as its own biases resulting from discretization error (Nabel et al., 2020; Fisher et al., 2018).

In this study, to demonstrate the impacts of disturbance and subgrid-scale heterogeneity on C and energy fluxes, we implement a dynamic tiling scheme in CLASSIC. Our implementation is a modified version of approaches that use a fixed number of tiles to represent age classes within the stand and may apply to other tile-based LSMs. We build upon a version of CLASSIC tailored to the pan-Canadian domain using region-specific plant functional types (PFTs) and a 0.22° ($\sim 20 \text{ km} \times 20 \text{ km}$) common grid (Curasi et al., 2023b). The age classes within the stand are represented using a variable number of subgrid tiles of variable fractional area and are subject to a user-determined maximum number of tiles available for the simulation. Tiles are split to represent disturbance and the resulting age and size structures. Tiles, and their underlying characteristics, are joined by the simulation either when the number of tiles reaches the user-determined maximum bound or pre-emptively based upon other user-determined parameters. The model is driven by externally forced harvest and fire from region-specific disturbance history drivers. We set an optimal maximum number of tiles that are available for the simulation by evaluating different model setups through model-on-model evaluation and assessing the run times of these setups. Finally, we compare the differences across runs to assess the impacts of the imposed trade-off between run time and a more detailed representation (i.e., more tiles). This investigation provides insight into the model configuration and the roles of fire, harvest, and tiling within CLASSIC as a step towards a comprehensive process-based assessment of Canada's terrestrial C cycle. These insights may also apply to other tile-based LSMs.

2 Methods

2.1 Study area

We use all of Canada south of 76° N as our simulation study area. Canada contains 650 Mha of forested land, and 98 Mha (18 %) of this forested land was disturbed from 1985–2015. On average, each year, 1.61 Mha is disturbed by wildfire, whereas 0.64 Mha is disturbed by harvest (Hermosilla et al., 2019). Disturbance due to wildfire is most prevalent in northern boreal regions, whereas harvest and other anthropogenic disturbances are more common in southern boreal regions where wildfire is suppressed. The spatial extent of individual disturbances is highly variable. In Canada, over the course of a year, each contiguous timber harvest event clears on average $98 \pm 115 \text{ ha}$. These timber harvest patterns are heavily influenced by forest management practices (Hermosilla et al., 2015b; White et al., 2017). Similarly, over the course

of a year, each contiguous fire event burns $324 \pm 633 \text{ ha}$ (Hermosilla et al., 2015b). The spatial scale of these change objects, sourced from 30 m spatial resolution Landsat imagery, falls well below the $\sim 40\,000 \text{ ha}$ resolution of the 0.22° pan-Canadian domain model grid. Located largely in southern latitudes, around 52 % of Canada's forested land is considered managed forest (Stinson et al., 2011). Canada's forest structure is characterized by relatively young stands in central and northwestern Canada, with much older stands found in the Pacific coastal and interior forests in British Columbia (Maltman et al., 2023). Forest ages in Canada are the result of prevailing natural disturbance regimes and, to a lesser extent, forest management practices (Pan et al., 2013).

2.2 The CLASSIC model

CLASSIC is an open-source community model that couples the Canadian Land Surface Scheme (CLASS) (Verseghy, 2000, 2017; Verseghy et al., 1993; Verseghy, 2007) and the Canadian Terrestrial Ecosystem Model (CTEM) (Melton and Arora, 2016; Arora, 2003). CLASSIC v1.0 is described and evaluated by Melton et al. (2020) and Seiler et al. (2021). A detailed description of model updates and improvements to CLASSIC since v1.0 that are utilized by our simulations can be found in Asaadi et al. (2018), MacKay et al. (2022), and Curasi et al. (2023b). We carry out simulations of the pan-Canadian domain using a parameterization of the model which includes Canada-specific plant functional types (PFTs) that were developed and evaluated by Curasi et al. (2023b).

The CTEM dynamic vegetation sub-model simulates photosynthetic fluxes at a 30 min time step in offline simulations and the allocation of C within live vegetation to structural and non-structural components of leaves, stems, and roots at a daily time step. CTEM also simulates daily autotrophic respiration from leaves, stems, and roots and heterotrophic respiration fluxes from litter and soil C. The pan-Canadian parameterization of CTEM utilizes 14 biogeochemical PFTs (Curasi et al., 2023b). CTEM is coupled to CLASS at a daily time step and provides CLASS with vegetation height, leaf area index, biomass, and rooting depth. CLASS, in turn, provides CTEM with mean daily soil moisture, soil temperature, and net radiation incident on the land surface. CLASS simulates ground and canopy energy exchange from four possible subareas – bare ground, snow-covered bare ground, canopy-covered ground, and snow-covered canopy – at a 30 min time step. It uses 20 ground layers from 0.1 to 30 m thick to a depth of over 61 m and simulates heat transfer within all permeable soil layers and the underlying bedrock. It also simulates water fluxes between the soil layers up until the depth of the impermeable bedrock layer. The depth of the impermeable bedrock layer in each grid cell is derived from Shang-guan et al. (2017). CLASS models a single-layer canopy and uses five physics PFTs, which map directly onto the

14 CTEM biogeochemical PFTs, in the pan-Canadian parameterization (Curasi et al., 2023b).

2.3 Dynamic tile representation of externally forced fire and harvest

2.3.1 The composite versus mosaic representation in CLASSIC

CLASSIC can utilize either a composite (one tile) or mosaic (> 1 tile) representation of the land surface. The composite representation simulates average individual PFTs for each grid cell and uses their average structural attributes (i.e., leaf area index, height, and rooting depth) to simulate the energy balance and physical environment (i.e., soil temperature). The structural attributes of all of the average individual PFTs that exist within a grid cell are averaged in proportion to their fractional coverages, and the PFTs all experience a common land surface physical environment. For the composite representation, a disturbance event (i.e., wood harvest) takes an amount of C from the average individual PFT pools that is proportional to the areal fraction disturbed (i.e., a complete harvest of 50 % of the grid cell thereby removes 50 % of the vegetation biomass; Fig. 1).

The mosaic representation splits the grid cell into multiple tiles representing fractional areas of the grid cell. Each tile receives the same meteorological forcing but simulates its respective average individual of each PFT present, PFT structural attributes, and energy balance. The structural attributes of all the average individual PFTs that exist within each tile are averaged in proportion to their fractional coverages, and the PFTs all experience a land surface physical environment common to that tile. The tiles are aggregated to the scale of the final model grid by accounting for each tile's fractional coverage of the grid cell. CLASSIC's tiling capability has been used in the past to investigate the impacts of subgrid-scale heterogeneity in soil texture by breaking grid cells with heterogeneous soil textures into tiles (Melton et al., 2017), as well as vegetation cover (Melton and Arora, 2014; Li and Arora, 2012) and competition between plant functional types (Shrestha et al., 2016) by breaking grid cells with heterogeneous vegetation cover into tiles. These approaches result in regional differences in fluxes of up to 30 %. We adapt the mosaic representation to dynamically create disturbance history tiles and represent the subgrid-scale heterogeneity resulting from disturbance (i.e., we represent a complete harvest of an area corresponding to 50 % of the grid cell as a 100 % reduction of the vegetation biomass in a new subgrid tile that covers 50 % of the grid cell; Fig. 1). In our approach, the tiles serve to represent vegetation that is in different stages of recovery. Thus, the soil textures and vegetation fractional cover are the same for all tiles within a given grid cell.

2.3.2 Notation and background

We present generalized equations that illustrate the dynamic tiling calculations done by the model to split and join tiles. In these equations, scalars are lowercase letters (i.e., $x = [1]$), vectors are bold lowercase letters (i.e., $\mathbf{x} = [x_1, x_2, \dots, x_n]$), and matrices are bold uppercase letters (i.e., $\mathbf{X} = (x_{1,1} \dots x_{1,n} \dots x_{n,1} \dots x_{n,n})$). The model is set up to simulate state variables for a user-defined maximum number of tiles within a grid cell (i.e., the state variable \mathbf{x}_{all} with a length equal to the user-determined maximum number of tiles). Tiles can be set as either active or inactive at each time step (Fig. 1). When the model identifies active tiles for merging or splitting (e.g., Sects. 2.3.4–2.3.6), they become candidate tiles. Depending upon the operation and the fraction of the grid cell involved, anywhere between one and the total number of tiles being actively simulated are candidate tiles for the merging or splitting operation. Because the maximum number of tiles is fixed, the model must manage the number of tiles being actively simulated. The model ensures that up to two inactive tiles are available to simulate disturbance each year (i.e., one for fire and one for harvest; see Sect. 2.3.4). During the merging or splitting operation, the model temporarily stores values from the candidate tiles before the operation (i.e., \mathbf{x}_{pre} of length n , the total number of candidate tiles) and after the operation (i.e., \mathbf{x}_{post} of length n , the total number candidate of tiles) and uses them to calculate the values for a new single output tile (i.e., x_{new}). All these values are temporarily stored and used in calculations up until the point where the dynamic tiling operation is complete, and the model's main data structures are updated.

2.3.3 Dynamic tiling splits and joins

Dynamic tiling allows the model to split grid cells into subgrid tiles during the model run or to join existing subgrid tiles. Dynamic tiling operations (splitting/joining) occur on 1 January at an annual time step alongside rigorous checks to ensure water, mass, and energy conservation. The area occupied by a given tile is a fraction of the grid cell land area between 0 and 1 (i.e., \mathbf{a}_{all} with a length equal to the user-determined maximum number of tiles). The sum of \mathbf{a}_{all} for all the active tiles within a grid cell must equal 1. When tiles are split, the fractional area occupied by the single new tile (a_{new}) must be less than the sum of the vector of fractional areas of the candidate tiles (\mathbf{a}_{pre} of length n candidate tiles). The candidate tiles' fractional areas are a product of the dynamic tiling operations that occur in all previous time steps. When the first dynamic tiling operation in a run occurs, $\mathbf{a}_{\text{pre}} = [1]$, but \mathbf{a}_{pre} is a much more complex vector in subsequent operations (e.g., $\mathbf{a}_{\text{pre}} = [0.1, 0.2, 0.3]$). The candidate tiles are later assigned a vector of new fractional areas adjusted to account for the new tile and the decrease in size of the candidate tiles (\mathbf{a}_{post} , also of length n candidate tiles;

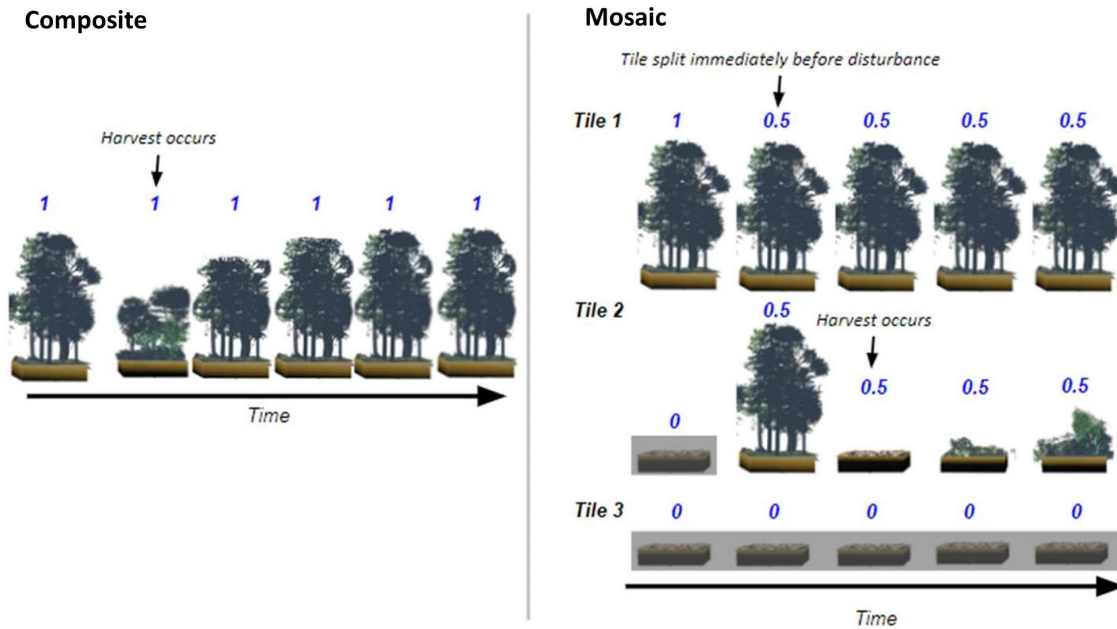


Figure 1. Illustrative diagram contrasting the composite (one tile) and mosaic (> 1 tile) representations of disturbance implemented herein. A hypothetical scenario where 50 % of a grid cell undergoes timber harvest is assumed here. The fraction of a grid cell that is occupied by a tile is denoted above each tile. Tiles that are not active have a gray background (e.g., tile 3 across all time steps).

Eq. 1).

$$a_{\text{new}} < \sum_{i=1}^n a_{\text{pre},i}$$

$$a_{\text{post},n} = a_{\text{pre},n} - a_{\text{new}} \frac{a_{\text{pre},n}}{\sum_{i=1}^n a_{\text{pre},i}} \quad (1)$$

When tiles are joined by the model, the fractional area of the new tile is the sum of the vector of the fractional areas of the candidate tiles. The candidate tiles are later assigned fractional areas of zero (Eq. 2).

$$a_{\text{new}} = \sum_{i=1}^n a_{\text{pre},i}$$

$$a_{\text{post}} = 0 \quad (2)$$

For a tile or group of tiles to be split or joined, they must pass rigorous checks that ensure they share the same abiotic characteristics and static fractional PFT cover. These characteristics (i.e., soil texture, soil permeable depth, and PFT fractional coverage) are copied directly to the new tile by the split or join. Mass-based variables (i.e., vegetation C pool mass, soil C pool mass, soil water, ponded water, and water held in the vegetation canopy) are split or joined using fractional-area-based weighted averages to ensure mass balance. The value of the mass-based variable in the new tile (M_{new} for l layers and o PFTs; kg m^{-2}) is the average of the values for the candidate tiles (M_{pre} of length n candidate tiles for l layers and o PFTs; kg m^{-2}) weighted by the fractional areas of the candidate tiles (Eq. 3).

$$m_{\text{new},lo} = \frac{\sum_{i=1}^n m_{\text{pre},ilo} a_{\text{pre},i}}{\sum_{i=1}^n a_{\text{pre},i}} \quad (3)$$

Temperature-based variables (i.e., the temperatures of the vegetation canopy, ponded water, snowpack, and soil) are split or joined using a fractional area-based weighted average that blends the different temperature materials from the candidate tiles. The value of a given temperature for the new tile (t_{new} for l layers; K) is a function of the temperatures in the candidate tiles (T_{pre} of length n candidate tiles for l layers; K) weighted by the fractional areas of the candidate tiles before the split, the masses of the pools which track that temperature (M_{pre} of length n candidate tiles for l layers and m pools; kg m^{-2}), and the specific heat capacities which characterize those mass pools (c for m pools; $\text{J kg}^{-1} \text{K}^{-1}$; Eq. 4).

$$t_{\text{new},l} = \frac{\sum_{i=1}^n \left(t_{\text{pre},il} a_{\text{pre},i} \sum_{j=1}^m (m_{\text{pre},ilj} c_j) \right)}{\sum_{i=1}^n \left(a_{\text{pre},i} \sum_{j=1}^m (m_{\text{pre},ilj} c_j) \right)} \quad (4)$$

2.3.4 Dynamic tiling management

The maximum number of dynamic tiles in a given simulation is limited by a parameter set at the start of the model run. If this upper limit is reached, tiles are joined based on a similarity criterion. By default, the model selects the two tiles with the most similar vegetation heights and joins them. The model uses the vector of tile average vegetation heights (\bar{h} of length n for the total number of tiles; m) and calculates the absolute differences between all possible combinations of the elements therein (i.e., using the nested iterators $n1$ and $n2$). The resulting absolute difference matrix of tile average

vegetation heights ($\Delta\mathbf{H}$, a $n1$ total number of tiles by $n2$ total number of tiles matrix; m) is used to judge the similarity between tiles. The tile average vegetation height is a function of each PFT height (\mathbf{H} of length n , the total number of tiles, for o PFTs; m) and the PFT fractional coverage within the tile (\mathbf{F} of length n , the total number of tiles for o PFTs; Eq. 5; Fig. S1 in the Supplement). In the default case, the two tiles with the minimum $\Delta\mathbf{H}$ are joined when the maximum number of dynamic tiles is reached.

$$\Delta_{n1,n2} = |n1 - n2|$$

$$n = \frac{\sum_{o=1}^{\# \text{ of PFTs}} h_{n,o} f_{n,o}}{\sum_{o=1}^{\# \text{ of PFTs}} f_{n,o}} \quad (5)$$

An optional relative height threshold (rht ; unitless) allows for tiles to be pre-emptively joined at a yearly time step before the maximum number of dynamic tiles is reached. rht can be conceptually thought of as breaking the tiles into equally spaced bins organized by vegetation height. It is used to calculate a threshold value from the maximum tile average vegetation height (\bar{h} ; m). The threshold logically determines which pairs of tiles are pre-emptively joined at a yearly time step based on the absolute differences in their tile average vegetation heights ($\Delta\mathbf{H}$; m ; Eq. 6; Fig. S1).

$$\Delta\mathbf{H} < \text{rht} \cdot \max(\bar{h}) \quad (6)$$

When the rht parameter is used, the optional tile preservation parameter (tpp ; number of tiles) prevents tiles with the shortest average vegetation height from being merged. tpp is an integer which determines the number of tiles that the model will retain, starting from the tile with the shortest average vegetation height. This means the tiling scheme will carry out pre-emptive joins based upon rht while preserving young recently disturbed tiles and explicitly representing early successional differences in fluxes (Bellassen et al., 2010; Zahle et al., 2006; Nabel et al., 2020). When dynamic tiling is active, the time since disturbance is tracked for all tiles. Time since disturbance increases at the CTEM time step (i.e., daily). Any disturbance event applied to a particular tile resets its time since disturbance to zero.

2.3.5 Externally forced fire

Externally forced fire builds upon the pre-existing fire module within CLASSIC (Melton and Arora, 2016; Arora and Melton, 2018). The annual fractional burned area in a grid cell is read from a file. The model assumes that fire impacts all non-crop PFTs.

If dynamic tiling is not active, biomass from the average individual and the litter pool burns proportional to the requested fractional burned area. If dynamic tiling is active, a new tile with a fractional area equal to the fractional burned area is split from the active tiles within the grid cell and subsequently burned. Depending upon the requested fractional

burned area and the conditions in the grid cell, the model uses anywhere between one tile and the total number of tiles being actively simulated as candidate tiles for this splitting operation.

To determine the candidate tiles for this splitting operation, the model ranks the tiles based on their probability of fire (p of length n) conditional on the total above-ground biomasses available for burning (b of length n ; kg C m^{-2}). p is a linear function of the lower biomass threshold (0.4 kg C m^{-2}) under which fire cannot sustain itself and the upper biomass threshold over which fire has a probability of 1 (1.2 kg C m^{-2} ; Eq. 7) (Moorcroft et al., 2001; Kucharik et al., 2000; Melton and Arora, 2016).

$$p_n = \max \left[0, \min \left(1, \frac{b_n - 0.4}{1.2 - 0.4} \right) \right] \quad (7)$$

The model initially selects tiles with a p of 1 as candidate tiles to be split to yield the tile to be burned. However, if these selected tiles do not contain enough fractional area to simulate the fractional burned area requested, the model selects tiles with a p of less than 1 from largest to smallest (Fig. S1). Externally forced fire uses a single probability (p) to rank tiles, whereas CLASSIC's standard fire module uses three probabilities to calculate the burned area: the probability of fire conditional on the total aboveground biomasses available for burning, the combustibility of the fuel based on its moisture content, and the presence of an ignition source (Arora and Boer, 2005; Arora and Melton, 2018). We make this simplification here because the fractional burned area comes from a file and all the tiles within a grid cell experience the same driving meteorology, limiting differences in moisture content and ignition (Melton et al., 2017; Melton and Arora, 2014). With dynamic tiling either active or inactive, we calculate the C emissions to the atmosphere using pre-defined PFT-specific fire emission fractions for each live vegetation component (i.e., both structural and non-structural leaves, stems, and roots) as well as the litter pool (v ; Table 1). We calculate the quantity of live vegetation C transferred to the litter pool as a result of fire-related mortality using pre-defined PFT-specific mortality fractions (Θ ; Table 1). Externally forced fire does not impact crop PFTs, and thus their biomass never combusts nor experiences fire-related mortality.

2.3.6 Externally forced harvest

Harvest simulates the removal of biomass from the landscape because of logging activities and builds upon the pre-existing land use change module within CLASSIC (Arora and Boer, 2010). The annual fractional harvested area on a per-grid-cell basis is read from a file. The model assumes that all harvest events are clearcuts that impact some fraction of the simulated grid cell.

If dynamic tiling is not active, the average individual is harvested proportional to the requested fractional area. If dy-

Table 1. The PFT-specific fire emission fractions (ν) used to calculate C emissions to the atmosphere due to fire for each live vegetation component (i.e., both structural and non-structural leaves, stems, and roots) and the litter pool as well as the PFT-specific mortality fractions (Θ) used to calculate the quantity of C from each live vegetation component transferred to the litter pool. Crop PFTs are not impacted by fire and are therefore not assigned fractions (Melton and Arora, 2016).

PFT type	Green leaves		Brown leaves		Stems		Roots		Litter
	Combusted (ν_L)	Litter (Θ_L)	Combusted (ν_B)	Litter (Θ_B)	Combusted (ν_S)	Litter (Θ_S)	Combusted (ν_R)	Litter (Θ_R)	Combusted (ν_D)
Tree	0.42	0.20	–	–	0.12	0.60	0.00	0.10	0.30
Herbaceous	0.48	0.10	0.54	0.06	0.00	0.00	0.00	0.25	0.42
Shrub	0.42	0.20	–	–	0.12	0.60	0.00	0.10	0.36

Table 2. The fractions of harvest-affected biomass transferred to different wood product pools for herbaceous PFTs and woody PFTs (ϵ). The fractions for woody PFTs differ depending on the aboveground biomass density (Arora and Boer, 2010).

	Aboveground biomass density (kg C m^{-2})	Fraction of deforested biomass emitted to the atmosphere (ϵ_A)	Fraction of deforested biomass as slash/pulp and paper products (ϵ_D)	Fraction of deforested biomass as durable wood products (ϵ_S)
Woody PFTs	> 4.0	0.15	0.70	0.15
	1.0–4.0	0.30	0.70	0.00
	< 1.0	0.45	0.55	0.00
Herbaceous PFTs	–	0.45	0.55	0.00

dynamic tiling is active, a new tile with a fractional area equal to the requested fractional area is split from the oldest undisturbed active tile, and the entire new tile is harvested. If the harvested area requested exceeds the fractional area of the oldest undisturbed active tile, the model selects additional active tiles as candidate tiles from oldest to youngest until there is sufficient fractional area.

In either case, the harvested aboveground biomass (i.e., both non-structural and structural stem and leaf C) is split into three streams using fractions developed by Arora and Boer (2010). These streams contribute C to the atmosphere, the slash/pulp and paper product pool, and the durable wood product pool. The fractions of harvested aboveground biomass allocated to each stream (ϵ ; Table 2) depend upon whether the PFT is woody or herbaceous and, in the case of woody PFTs, the aboveground biomass density. Unlike the procedure described by Arora and Boer (2010) where root biomass is transferred to the slash/pulp and paper product pool, we transfer harvested root biomass to the applicable PFT and soil-depth-specific litter pools.

2.4 Model forcing

2.4.1 Meteorological drivers and land cover

CLASSIC requires seven meteorological forcing variables: incoming shortwave radiation, incoming longwave radiation, air temperature, precipitation rate, air pressure, specific humidity, and wind speed. We use the interpolated and disaggregated meteorological forcing described in detail by Meyer

et al. (2021) and Curasi et al. (2023b) (GSWP3–W5E5–ERA5) in our simulations. The 1901–1978 portion of the forcing comes from the Inter-Sectoral Impact Model Inter-comparison Project GSWP3–W5E5 and the 1979–2018 portion comes from the ERA5 time series bias-corrected to match the means of the overlapping period in the GSWP3–W5E5 (Kim, 2017; Lange, 2019, 2020a, b; ECMWF, 2019). The atmospheric CO₂ concentrations (1700–2017) were obtained from the global carbon project (“Trends in atmospheric carbon dioxide”, National Oceanic & Atmospheric Administration, Earth System Research Laboratory (NOAA/ESRL), 2022; Friedlingstein et al., 2022).

We set the fractional coverage of PFTs using the remotely sensed 14 PFT-hybrid land cover product generated by Wang et al. (2023) and expanded upon and evaluated by Curasi et al. (2023b). This land cover corresponds to the year 2010. This land cover product combines information from the North American Land Change Monitoring System land cover (Latifovic et al., 2017), the National Terrestrial Ecosystem Monitoring System (NTEMS) (Hermosilla et al., 2018, 2016), satellite-derived maps of the National Forest Inventory attributes (Beaudoin et al., 2018), and British Columbia’s biogeoclimatic ecosystem classification map (MacKenzie and Meidinger, 2018; Salkfield et al., 2016). Using a land cover that does not vary in time (i.e., static land cover as opposed to dynamic or prescribed land cover changes) allows us to focus on the influences of fire, harvest, and dynamic tiling on the model outputs.

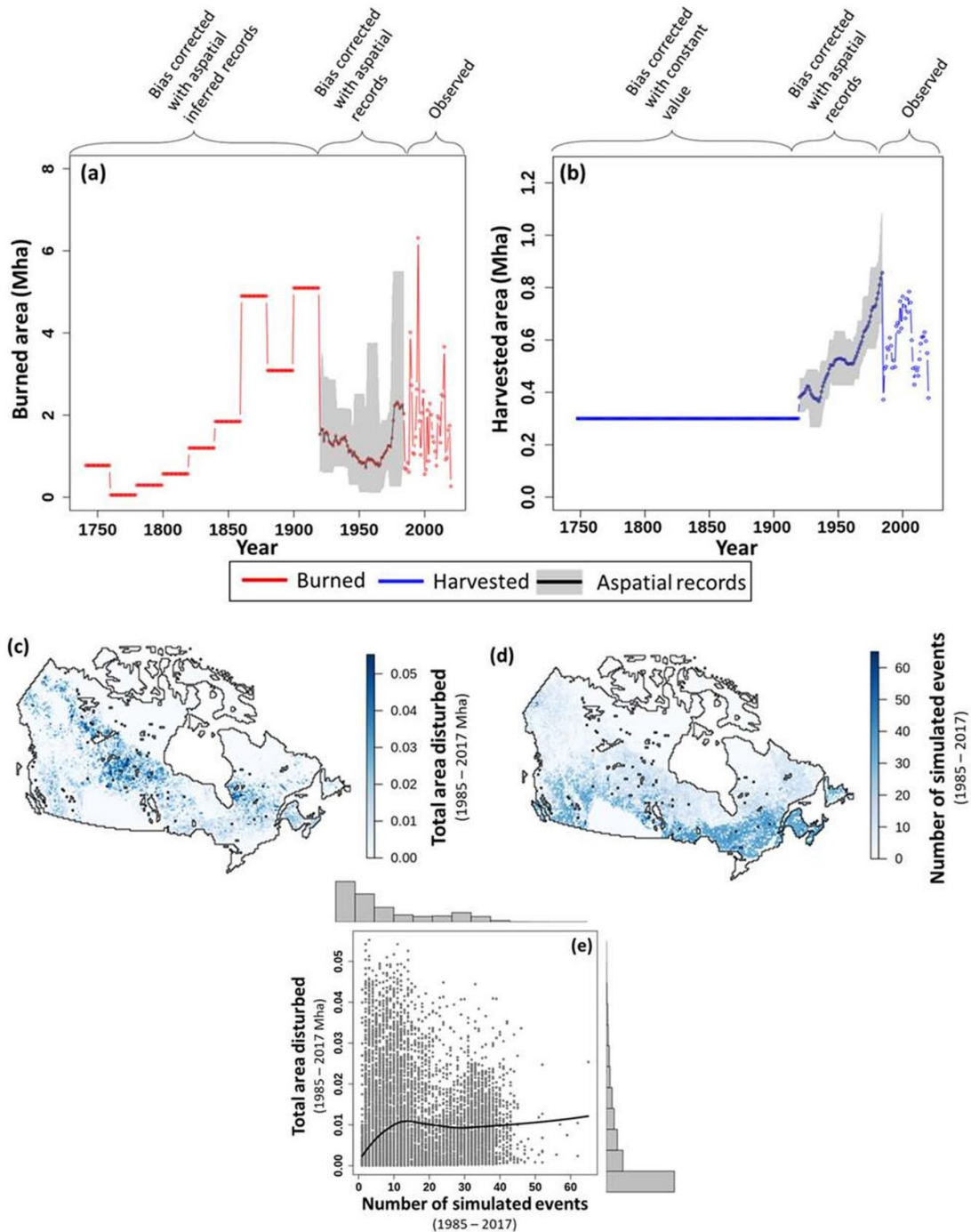


Figure 2. Plots of the disturbance drivers over time. Annual total (a) burned and (b) harvested areas from 1740–2020. “Observed” indicates the period that uses the Landsat fire and harvest observations (Hermosilla et al., 2016, 2015a, b). “Bias-corrected with aspatial records” indicates the period where the disturbance was inferred from the 2019 stand age (Maltman et al., 2023) and bias-corrected using the aspatial harvested and burned areas (Skakun et al., 2021; World Resources Institute, 2000; Van Wagner, 1988). “Bias-corrected with aspatial inferred records” and “Bias-corrected with constant value” indicate the period where the inferred disturbance was bias-corrected based on Kurz et al. (1995) and Chen et al. (2000), respectively. The aspatial records line is the 9-year running mean, min, and max of the aspatial total harvested and burned area data sets. (c) Per-grid-cell total area disturbed (1985–2017) and (d) the total number of simulated events (1985–2017). (e) Per-grid-cell total area disturbed, excluding undisturbed cells, plotted against the total number of simulated events. The black line is a LOESS curve. Note that a simulated event combines all the individual fire or harvest events that occur in a grid cell in a single year, with a maximum of two simulated events per year (one fire and one harvest) occurring in each grid cell.

2.4.2 Fire and harvest forcing

We develop fire and harvest drivers that detail the per-grid-cell annual fractional area harvested or burned between 1740 and 2017 (Fig. 2a and b). For the satellite era (1985–2017), we use remotely sensed 30 m spatial resolution records of harvest and fire events. These data were derived from Landsat by using breakpoint detection to identify changes and trends (Hermosilla et al., 2016, 2015a) followed by a random forest classification of change types (Hermosilla et al., 2015b). We mask the remotely sensed harvest records to include only private, long-term tenure, and short-term tenure forests, as indicated by Stinson et al. (2019).

Before the availability of remotely sensed records used herein (pre-1984), to our knowledge, there are no spatially explicit pan-Canadian integrated harvest and fire data sets available. Therefore, to represent the impact of historical disturbance on the model state, we employ established methods for inferring disturbance events from stand age (Nabel et al., 2020; Kurz et al., 2009; Chen et al., 2000, 2003). We also focus our analysis of the CLASSIC simulations on the satellite era (1985–2017) due to uncertainties in inferred historical disturbance and the model state before the satellite era. Maltman et al. (2023) derived a 30 m resolution stand-age map for 2019 from Landsat and MODIS data utilizing three methods. The methods included disturbance detection for stands between 0 and 34 years of age, the detection of spectral signals indicative of recovery for stands between 34 and 54 years of age, and inverting allometric equations for stands between 54 and 150 years of age. We infer the year in which the last disturbance occurred from the stand age. For example, a 40-year-old forest in 2019 is assumed to have been last disturbed in 1979. We use regional averages of the per-pixel ratio of burned to total disturbed area from the first decades of the satellite era (1985–1995) to fraction total inferred disturbance into fire and harvest.

However, pre-1984 disturbance that has been inferred from stand age does not align with available aspatial records of total harvested and burned area within Canada. Therefore, we utilize the aspatial records to bias-correct the 1740–1984 disturbance that has been inferred from stand age to ensure that the total values match the available historical records. From 1740–1920, we utilized aspatial records of total disturbed area derived from 1920 stand age with harvest held constant (0.3 Mha yr^{-1}) (Chen et al., 2000; Kurz et al., 1995). From 1920–1984, we utilized aspatial records of the total harvested and burned area within Canada from Skakun et al. (2021) and World Resources Institute (2000). We utilize bias correction that retains the spatial patterns of pre-1984 disturbance inferred from stand age while correcting positive and negative biases to match the aspatial records. This necessitated two distinct bias correction methods. For years with positive biases, the positive bias indicates that sufficient disturbance is inferred from stand age. In these cases, a uniform bias correction factor can be used to scale down disturbance.

Years with negative biases, however, do not contain sufficient disturbance as inferred from stand age. Here, residual disturbed area from nearby years needs to be added to the year under consideration to match the aspatial records' level of disturbance while preserving the spatial patterns derived from stand age. Because the uncertainty of stand age estimates increases further into the past, the negative bias correction is carried out starting in 1984 and looping backward annually until 1740 (Maltman et al., 2023).

First, for years in which burned or harvested area inferred from stand age ($\mathbf{D}_{\text{inferred}}$ for i years, l grid cells; m^2) exceeded the aspatial records ($\mathbf{d}_{\text{aspatial}}$ for i years; m^2), we correct the positive biases. We calculate an aspatial bias correction factor (f for i years; unitless; Eq. 8).

$$f_i = \frac{\left(\left(\sum_{l=1}^{\# \text{ of grid cells}} \mathbf{d}_{\text{inferred},i,l} \right) - \mathbf{d}_{\text{aspatial},i} \right)}{\left(\sum_{l=1}^{\# \text{ of grid cells}} \mathbf{d}_{\text{inferred},i,l} \right)} \quad (8)$$

Because the pre-1985 records are aspatial, the bias correction factor is temporally explicit but uniformly applied across space. When we apply the bias correction factor to the inferred disturbance time series, the result is a new time series with all the positive biases corrected ($\mathbf{D}_{\text{downsc}}$ for i years, l grid cells; m^2 ; Eq. 9).

$$\mathbf{d}_{\text{downsc},il} = \mathbf{d}_{\text{inferred},il} - \mathbf{d}_{\text{inferred},il} f_i \quad (9)$$

When we apply the bias correction factor, we retain the spatially and temporally explicit residuals ($\mathbf{D}_{\text{residual}}$ for i years, l grid cells; m^2 ; Eq. 10).

$$\mathbf{d}_{\text{residual},il} = \mathbf{d}_{\text{inferred},il} - \mathbf{d}_{\text{downsc},il} \quad (10)$$

Second, for years in which burned or harvested area inferred from stand age falls below that indicated in the aspatial records, we correct the negative biases by adding in the residuals from nearby years (Fig. 3). We loop backward in time from 1984 to 1740 and accumulate residuals ($\mathbf{r}_{\text{moving}}$ for l grid cells; m^2) extending as far back in time as needed to exceed the aspatial record for the year under consideration ($\mathbf{d}_{\text{aspatial},i}$). We calculate an aspatial bias correction factor (f ; unitless) and use it to apply a fraction of $\mathbf{r}_{\text{moving}}$ to the inferred disturbance time series and subtract the residuals used from $\mathbf{r}_{\text{moving}}$. When the spatially explicit residuals are exhausted (~ 1920 for fire only), they are replenished using the entire gridded remotely sensed and stand-age-inferred disturbance record. This procedure continues until all the negative biases have been corrected between 1984 and 1740, yielding the final spatially explicit time series ($\mathbf{D}_{\text{final}}$ for i years, l grid cells; m^2).

2.5 Simulation protocol

We carry out a total of 14 simulations using a common simulation protocol to investigate the impacts of differ-

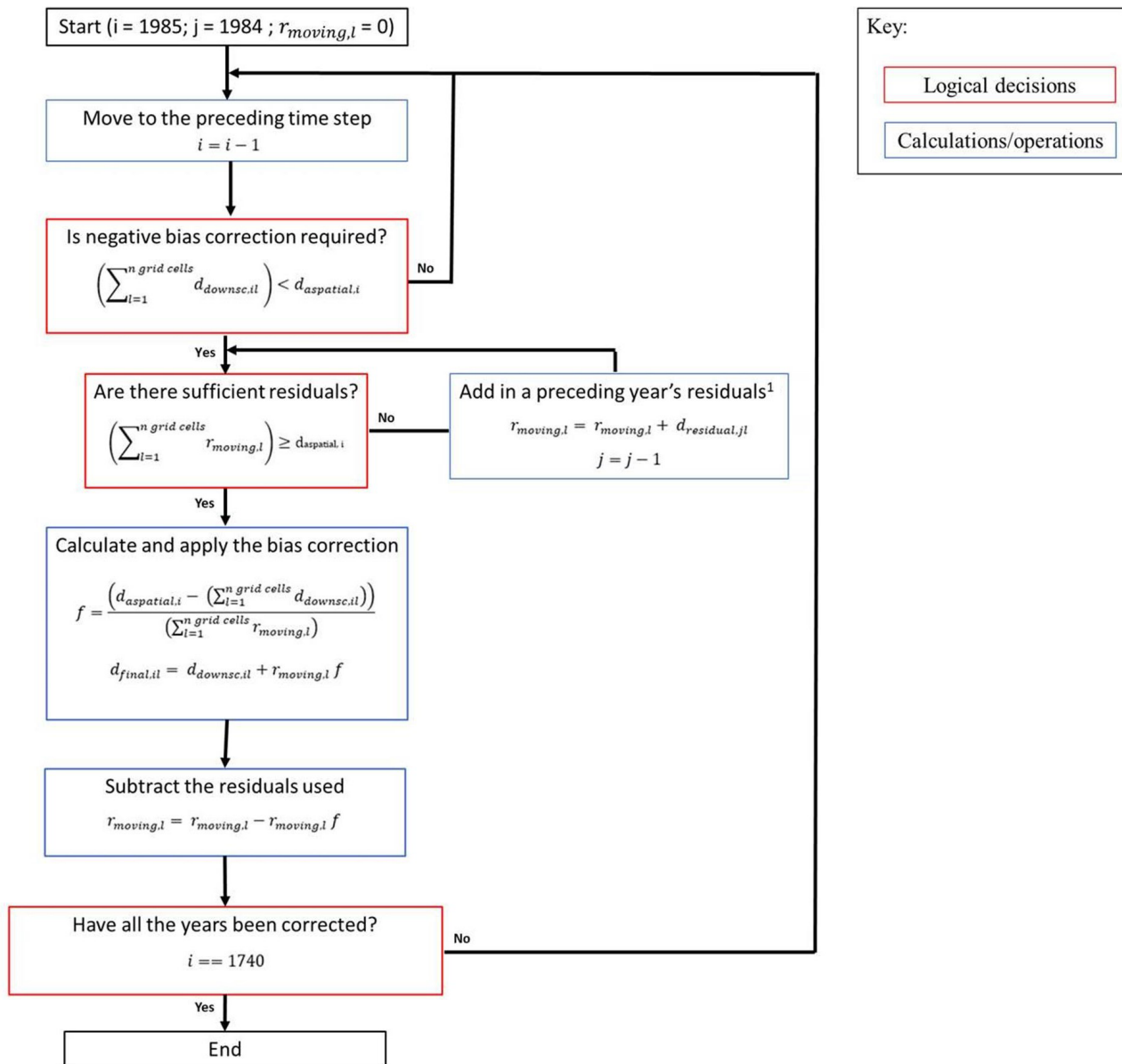


Figure 3. A schematic diagram of the negative bias correction algorithm with applicable equations and logical tests. ¹ Not shown: when the spatially explicit residuals are exhausted, they are replenished using the entire remotely sensed and stand-age-inferred disturbance record.

ent maximum numbers of available tiles, *rht*, and *tpp* (Table 3). *rht* (0.04–0.16, unitless) can be conceptually thought of as breaking the range of tile average vegetation heights into between 24 and six equally spaced bins, depending upon its value (e.g., (1 bin $\text{m m}^{-1}/6$ bins) = 0.16 m m^{-1}). *tpp* (4–6 tiles) can be conceptually thought of as the maximum number of discrete disturbance events that the model can simulate in a grid cell over 2–3 years (e.g., (1 harvest tile yr^{-1} + 1 fire tile yr^{-1}) \times 3 years \times 6 tiles).

We spin up the model to equilibrium conditions corresponding to the year 1700 and then do a transient run over the period 1700 to 2017. For the spin up, we loop the earliest

25 years of climate data available (1901–1925) and hold atmospheric CO_2 concentrations constant at the pre-industrial (1700) level. The 1700–1900 portion of the transient run uses the same loop of 1901–1925 climate but transient atmospheric CO_2 concentrations. The 1900–2017 portion of the transient run uses transient atmospheric CO_2 concentrations and evolving GSWP3–W5E5–ERA5 climate. During the full transient simulation from 1740–2017, the fire and harvest are applied (see Sect. 2.4). The 14 transient simulations utilize their individual, unique land-surface representation (i.e., composite or mosaic), maximum number of available tiles, *rht*, and *tpp* for the entire 1700–2017 run (Table 3).

Table 3. An overview of the simulations conducted in this study.

Abbreviation	Land surface representation	Includes disturbance	Max available tiles	Relative height threshold	Tile preservation parameter
1-tile/not-disturbed	Composite	No	1	–	–
1-tile/disturbed	Composite	Yes	1	–	–
3-tile	Mosaic	Yes	3	–	–
7-tiles	Mosaic	Yes	7	–	–
12-tile	Mosaic	Yes	12	–	–
18-tile	Mosaic	Yes	18	–	–
25-tile	Mosaic	Yes	25	–	–
32-tile	Mosaic	Yes	32	–	–
Optimal	Mosaic	Yes	12	0.04	4
–	Mosaic	Yes	12	0.08	4
–	Mosaic	Yes	12	0.16	4
–	Mosaic	Yes	12	0.04	6
–	Mosaic	Yes	12	0.08	6
–	Mosaic	Yes	12	0.16	6

The CLASSIC nitrogen cycling module is not active in these simulations (Asaadi and Arora, 2021; Arora and Boer, 2010).

2.6 Model evaluation

We carry out model-on-model comparisons for a selection of variables and model configurations for the satellite era portions of our simulations (1985–2017) to select the model setup that optimally balances a detailed process representation and model run time (Table 3). This model-on-model approach has the benefit of canceling out any pre-existing biases in the model and focusing our results on the impacts of subgrid-scale heterogeneity, and discretization error (similar to Torres-Rojas et al., 2022; Moorcroft et al., 2001). We also use these evaluations to demonstrate the relative impact of representing subgrid-scale heterogeneity within our modeling framework. We evaluate a suite of C cycling and surface-energy-balance-related variables, including the land carbon pool (cLand), vegetation C (cVeg), soil C (cSoil), gross primary productivity (GPP), autotrophic respiration (Ra), heterotrophic respiration (Rh), ecosystem respiration (ER), leaf area index (LAI), sensible heat flux (HFSS), latent heat flux (HFLS), albedo (ALBS), fire emissions (fFire), total deforested C (fDeforestTotal), and cumulative deforested C (the running sum of fDeforestTotal starting in 1985; fDeforestCumulative).

To select the optimal maximum number of tiles available for the simulation as well as the rht and tpp, we calculate the mean squared deviation (msd for the j model runs detailed in Table 3 over the 1985–2017 period) between the model runs under evaluation and the reference 32-tile run. The 32-tile run is the reference point, as it is the simulation with the least compromise between run time and simulation detail and is assumed to best represent the impacts of disturbance in CLASSIC. MSD represents the mean of the squared dif-

ferences between the annual summary (i.e., means for fluxes and sums for pools) of each variable for the 32-tile run ($\hat{x}_{32\text{tile}}$ containing i years) and that for the simulations under evaluation (\hat{X} containing i years for j model runs; Eq. 11).

$$\text{msd}_j = \frac{1}{33} \sum_{i=1985}^{2017} (\hat{x}_{j,i} - \hat{x}_{32\text{tile},i})^2 \quad (11)$$

We also use a normalized response metric ($\Delta\bar{X}_{\text{norm}}$ for j model runs, k variables; Eq. 12) to evaluate the relative impacts of disturbance and subgrid-scale heterogeneity on the simulations. The normalized response metric is a unitless summary statistic. Its strength is that a wide range of variables with different units can be visualized on the same axis to make relative comparisons of their simulated responses to disturbance and tiling. For a given variable, the metric normalizes each variable’s output (X for i years, j model runs, k variables, l grid cells) using the minimum and maximum across all the outputs (X_{norm} for i years, j model runs, k variables, l grid cells; Eq. 12). Each normalized variable is averaged across the model domain and run years (\bar{X}_{norm} for j model runs, k variables; 1985–2017) considering each model grid cell’s area ($a_{\text{grid cell}}$; m^2). Finally, the absolute value of the difference between \bar{X}_{norm} for the desired runs (the 1-tile/not-disturbed and 32-tile runs) and the 1-tile/disturbed run is calculated (Eq. 12).

$$x_{\text{norm},i,j,k,l} = \frac{(x_{i,j,k,l} - \min(X_k))}{(\max(X_k) - \min(X_k))} \quad (12)$$

$$\bar{x}_{\text{norm},j,k} = \frac{\sum_{i=1985}^{2017} \left(\sum_{l=1}^{\# \text{ of grid cells}} x_{\text{norm},i,j,k,l} a_{\text{grid cell},l} \right)}{33 \left(\sum_{l=1}^{\# \text{ of grid cells}} a_{\text{grid cell},l} \right)} \quad (13)$$

$$\Delta\bar{x}_{\text{norm},j,k} = \left| \bar{x}_{\text{norm},j,k} - \bar{x}_{\text{norm},1\text{-tile}/\text{disturbed},k} \right| \quad (14)$$

All plots are created using R or the External Dynamic and Interactive Framework Integrating CLASSIC Experiments (EDIFICE) Python suite (Hijmans et al., 2015; R Core Team, 2013).

3 Results and discussion

3.1 Disturbance events within Canada

For the period represented by satellite data in this study, the highest total disturbed areas are in central boreal regions of the country and are attributable to wildfire events (Fig. 2c). In contrast, harvest is concentrated on the west coast and in eastern boreal and maritime regions of the country. The annual total disturbed area differs widely between years during the satellite era (Fig. 2a and b). In aggregate, harvest occurs in $\sim 2\%$ of the land area modeled, and fire occurs in $\sim 6\%$ from 1985 to 2017. The total number of simulated disturbance events is moderate, with 89% of the grid cells incorporating 32 or fewer simulated disturbance events during the satellite era and 61% incorporating 11 or fewer (Fig. 2d and e). Our aspatial tiling scheme operates on an annual time step, and therefore the maximum number of possible events in the 1985–2017 drivers is 66 (i.e., a harvest and fire each year for 33 years; Fig. 2e). Generally, beyond 11 simulated disturbance events, there is a limited correlation between the number of simulated disturbance events and the total area disturbed (Fig. 2e).

3.2 Model parameterization

The change in the MSD (Fig. 4a–h) as the maximum number of available tiles for the run increases from 1 to 32 exhibits a roughly exponential decline for the surface energy balance (HFSS, HFLS) and C-cycle-related variables (cLand, GPP, ER, LAI). The MSD is near zero at 7–12 tiles. The 32-tile simulation captures all the discrete disturbance events from 1985–2017 across most of the model domain (Fig. 2). However, a simulation that resolves all the disturbance events between 1740 and 2017 as tiles would require far more than 32 tiles in many forested areas and would be computationally intractable. However, we infer from the exponential (e.g., rather than linear) decreasing rate of change in Fig. 4a–f that our reference 32-tile simulation has minimal discretization error and converges on the results of that computationally intractable simulation (Torres-Rojas et al., 2022; Nabel et al., 2020; Necedal and Wright 2006). The difference in MSD between the 32-tile simulation and that computational intractable simulation would likely be vanishingly small, similar to the difference between the 25-tile and 32-tile simulations (Nabel et al., 2020; Fisher et al., 2018; Ellner and Guckenheimer, 2011; Gelman and Hill, 2006). These roughly exponential declines in MSD reflect the model's ability to discretize patches of vegetation in different stages of recovery using greater numbers of tiles. This is reflected in how

the statistical distributions of aboveground tree biomass in forested grid cells change as more tiles are utilized in the simulation (Fig. 5a).

Disturbance-related variables, including fFire as well as fDeforestedTotal, exhibit a less sharp decline when going from one to seven tiles and approach zero at 12 tiles (Fig. 4g and h). This reflects the influence of selecting and splitting tiles in different phases of recovery on these processes and the extent to which recovering tiles with lower aboveground tree biomass are represented in the simulation (Fig. 5a). As a result, there is a discontinuity between representing these processes using average individuals, a small number of highly heterogeneous tiles, and many tiles (Figs. 4g and h and 5a). This pattern is also likely influenced by the relatively low magnitude of the differences between the simulations compared to the fluxes themselves (Fig. 6a, h, and i).

The run time for the satellite-era simulation (1985–2017) with one tile is ~ 318 CPU hours (i.e., the sum of time utilized by all cores across multiple machines; Xeon Platinum 8380). Compared to the 1-tile run, the 32-tile, 12-tile, and optimal runs consume 14 times, 3 times, and 2 times as many CPU hours, respectively. The run time of the simulations increases linearly between one and 12 tiles (Fig. 4i) but increases more rapidly from 18 to 32 tiles due to the increasingly large multidimensional per-tile structures in memory. The intercept (i.e., the overhead for pre-processing meteorological files and initializing message passing interface sessions to run the model with a single tile) is around 3 times the slope (i.e., the time required to run each additional tile) for simulations with less than 12 tiles. This suggests that the splitting operations involved in simulating additional tiles are computationally efficient and do not dramatically increase the run time (Nabel et al., 2020).

As with all modeling exercises, we must balance model accuracy, complexity, and computational efficiency. We, therefore, use simulations with 12 tiles to set the *rht* (i.e., the relative height threshold for pre-emptively joining tiles) and *tpp* (i.e., the number of preserved recently disturbed tiles) parameter values. Simulations using 12 tiles and different *rht* and *tpp* parameters are very similar in terms of run time, and the surface energy balance and C-cycle-related variables exhibit no consistent patterns (Fig. S2a–f and i). There is a gradual increase in MSD for fFire and fDeforestedTotal as *rht* and *tpp* increase (Fig. S2g–h). However, these differences are again of relatively low magnitude compared to the fluxes themselves (Fig. 6a, h, and i). Therefore, we chose an *rht* of 0.16 and a *tpp* of 4 to maximize computation efficiency. The optimal parameterization has MSD values similar to those of a run with 12 tiles but with a lower run time ($\sim 23\%$ less; Fig. 4i). The optimal model nearly approximates the heterogeneous tile structure of the more complex 32-tile simulation and represents forested areas with low aboveground tree biomass like the 32-tile simulation, in line with observations of aboveground tree biomass from the NFI (Fig. 5b). However, it may over-smooth the transition be-

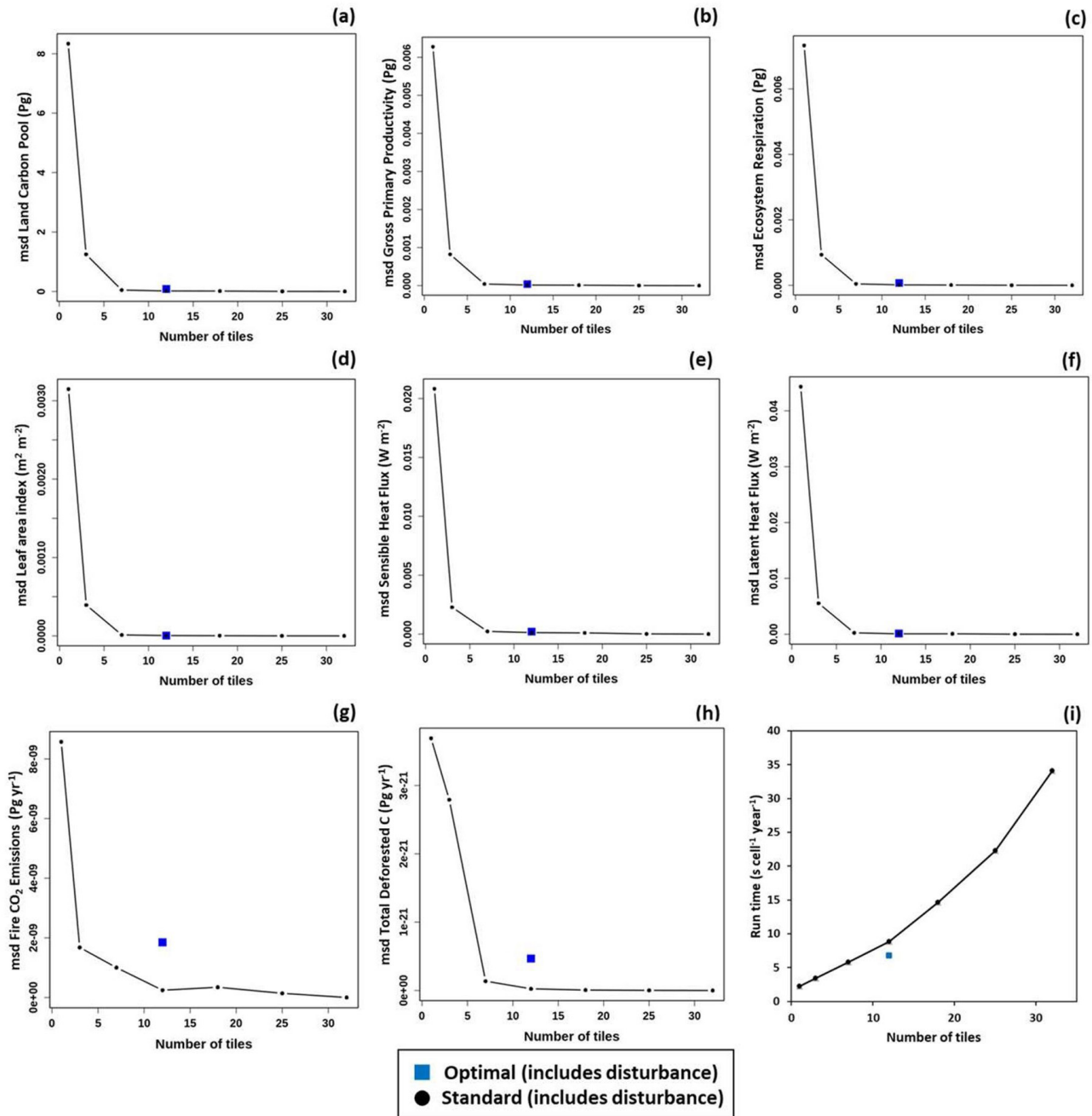


Figure 4. Plots of the mean squared deviation (msd; 1985–2017; Eq. 11) for (a) the land carbon pool (cLand), (b) gross primary productivity (GPP), (c) ecosystem respiration (ER), (d) leaf area index (LAI), (e) sensible heat flux (HFSS), (f) latent heat flux (HFSS), (g) fire emissions (fFire), and (h) total deforested carbon (fDeforestTotal) for model runs including disturbance with varying numbers of tiles (1–32) compared against the run including disturbance with the largest number of tiles (32). (i) The run time for each configuration. Values are also shown for the optimal model run including disturbance with 12 tiles (tile preservation parameter, $tpp = 4$; relative height threshold, $rht = 0.16$).

tween low- and high-biomass areas (i.e., the $\sim 2\text{--}3\text{ g C m}^{-2}$ range in Fig. 5b), thereby impacting the size classes of the tiles selected for splitting during the disturbance simulation (Fig. 4g and h). Nonetheless, the optimal simulation effectively balances computational efficiency and discretization error.

3.3 Impacts on simulated variables

The responses of the modeled variables to dynamic tiling (i.e., 1-tile/disturbed vs. 32-tile, as illustrated in Fig. 1, Table 3) often meet or exceed their responses to disturbance alone (i.e., 1-tile/not-disturbed vs. 1-tile/disturbed;

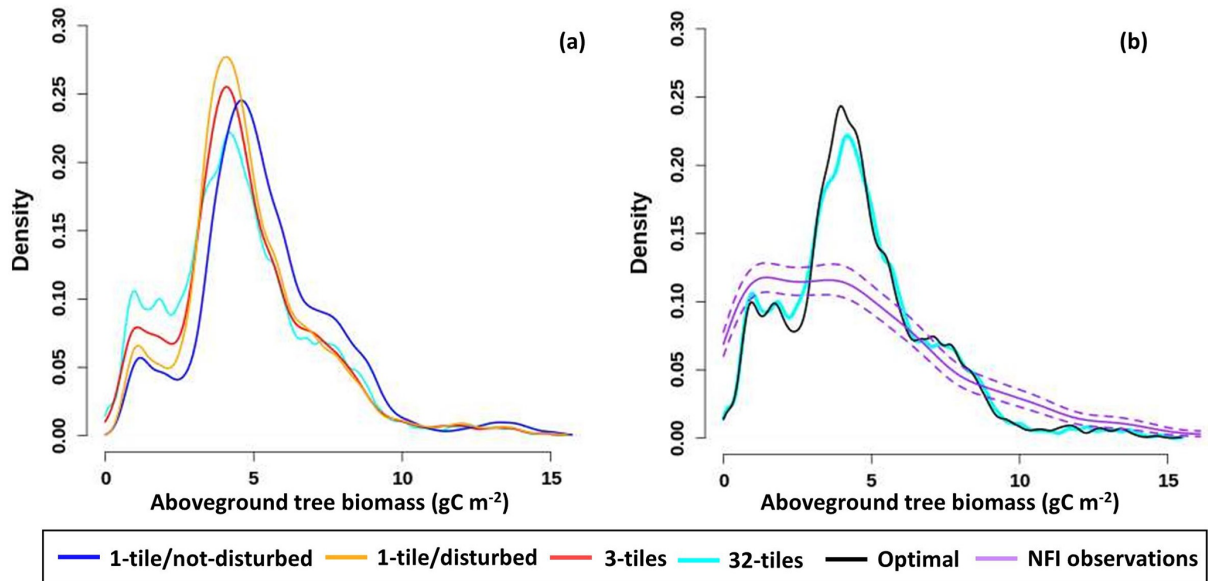


Figure 5. Weighted histogram of aboveground tree biomass for forested areas of Canada (a) at the end of a selection of model runs, including the 1-tile/not-disturbed run, 1-tile/disturbed, 3-tiles, and 32-tiles, as well as for (b) 32-tiles, optimal (12 tiles, four preserved tiles, and a threshold of 0.16), and observations from the National Forest Inventory (NFI) (Gillis et al., 2005). All runs using > 1 tile include disturbance. The bootstrapped 95 % CI for the NFI observations is also shown. The contributions of all forested subgrid areas weighted by their fractional area within the modeled region are considered. An area is classified as forested if it contains at least 50 % tree cover.

Fig. 6a). The impact of the optimal tiling scheme is minimal by comparison; therefore, we focus on comparisons between the 1-tile/not-disturbed, 1-tile/disturbed, and 32-tile outputs (Figs. 6b–i and S3). C-cycle-related variables, including cVeg and LAI, show the strongest responses to disturbance, whereas energy-balance-related variables, including HFLS, HFSS, and ALBS, show the weaker responses. Many variables also respond strongly to dynamic tiling, including LAI, Ra, and cVeg (Fig. 6a, b, and e). Select surface-energy-balance-related variables, including HFLS, HFSS, and ALBS, respond more strongly to dynamic tiling than disturbance alone (Fig. 6a). These strong responses further reinforce the impact of disturbance-induced subgrid-scale heterogeneity on ecosystem processes and the value of representing this heterogeneity within models (Bellassen et al., 2010; Zaehle et al., 2006; Nabel et al., 2020; Körner, 2006; Dore et al., 2010; Luyssaert et al., 2014; Erb et al., 2017).

Disturbance-related variables such as fFire exhibit little difference from subgrid-scale heterogeneity (Fig. 6h), whereas fDeforestCumulative increases slightly (Fig. 6i). These patterns occur as fire can potentially impact all subgrid stands above a certain biomass threshold (Eq. 7), while wood harvest preferentially impacts the tiles with the largest aboveground biomass (i.e., approximating the highest-quality tiles being harvested). Biomass removal by disturbance leads to an ~ 1.6 Pg decrease in cVeg across Canada (an 8 % decrease), while the subgrid-level (tiled) representation of these processes leads to another ~ 1 Pg decrease (Fig. 6b). LAI mirrors these patterns, with a 4 % decrease due to disturbance

and another 4 % decrease with the subgrid-level (tiled) representation (Fig. 6e). As a result of disturbance, cSoil decreases at a higher rate from 1985 to 2017, whereas cVeg increases at very similar rates of ~ 0.035 Pg yr⁻¹ (Fig. 6b and c). For GPP and Ra, the impact of dynamic tiling is ~ 1.5 – 2.5 times the impact of disturbance alone (Fig. 6a and d). This offset in GPP and Ra is, in part, likely a product of dynamic tiling simulating the naturally slower process of recovery from bare ground versus the recovery of an average individual with substantial pre-existing biomass and leaf area (Zaehle et al., 2006; Körner, 2006; Dore et al., 2010; Luyssaert et al., 2014). This slower recovery likely also contributes to the losses in cVeg between the 1-tile/disturbed and 32-tile simulation.

Dynamic tiling has impacts on HFLS, HFSS, and ALBS that are ~ 1.5 – 4 times the impact of disturbance alone (Fig. 6a). The relative impact on HFLS is the more muted of the three, possibly because, while removing vegetation causes a decrease in transpiration, evaporation from the ground surface increases (Fig. 6g). Dynamic tiling does appear to have larger impacts on ALBS, with the surface becoming brighter; by extension, HFSS decreases (Fig. 6a and f). This occurs as the model with dynamic tiling is capable of representing sparsely vegetated and often snow-covered fractions of the land surface as a result of recent disturbance (Bright et al., 2013; Nabel et al., 2020). These impacts are muted or absent when disturbance is simulated by an average individual model because only a proportion of the average individual's biomass is removed, with enough

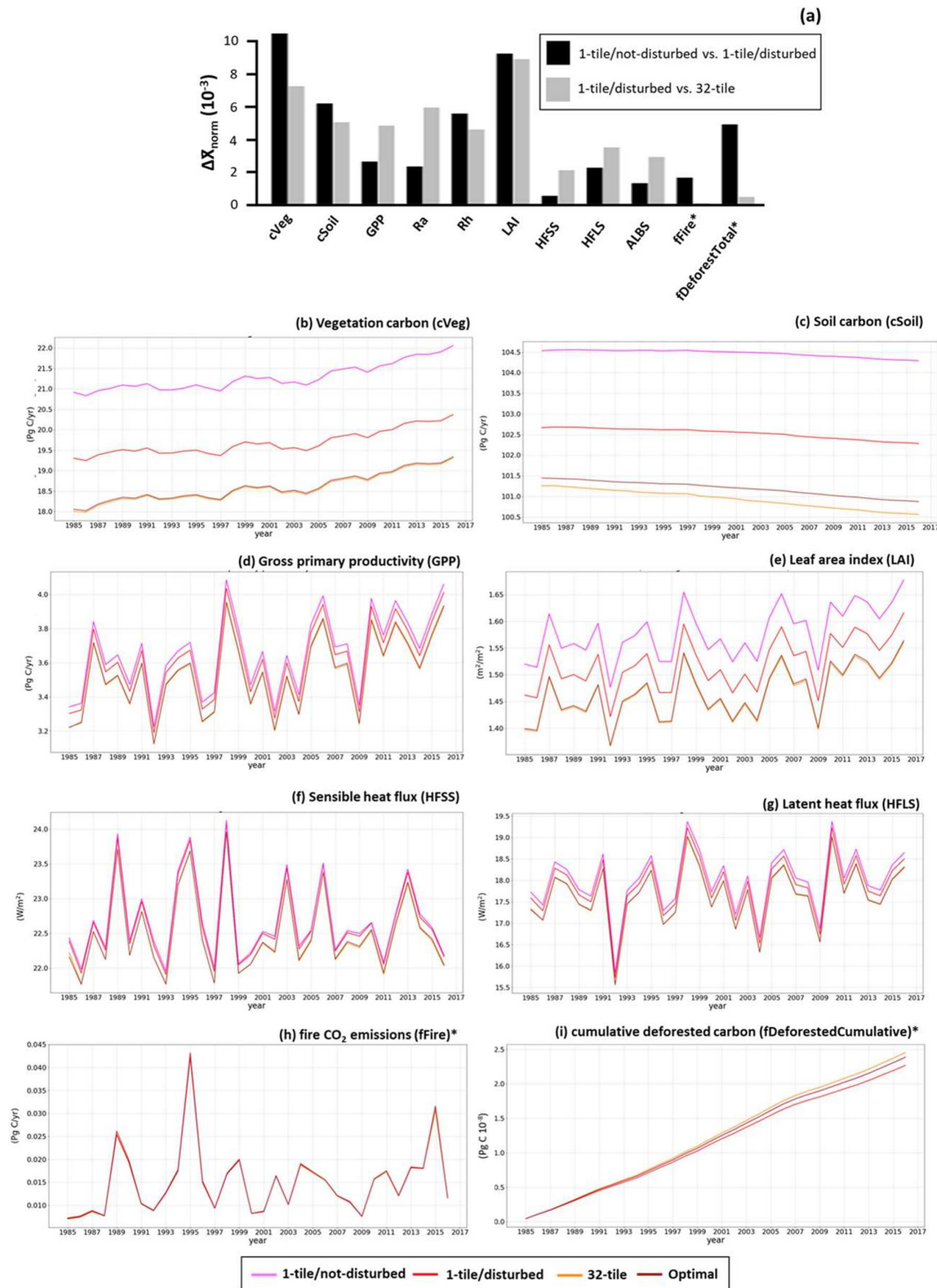


Figure 6. (a) Plot of the normalized response metric ($\Delta \bar{X}_{norm}$; Eq. 12) for 1-tile/not-disturbed versus 1-tile/disturbed and for 1-tile/disturbed versus 32-tile for vegetation carbon (cVeg), soil carbon (cSoil), gross primary productivity (GPP), autotrophic respiration (Ra), heterotrophic respiration (Rh), leaf area index (LAI), sensible heat flux (HFSS), latent heat flux (HFLS), albedo (ALBS), fire emissions (fFire), and total deforested carbon (fDeforestTotal). Time series plots of (b) cVeg, (c) cSoil, (d) GPP, (e) LAI (f) HFSS, (g) HFLS, (h) fFire, and (i) cumulative deforested carbon (fDeforestCumulative; the running sum of fDeforestTotal starting in 1985) for 1-tile/not-disturbed, 1-tile/disturbed, 32-tile, and optimal (tpp = 4; rht = 0.16; purple). All runs using > 1 tile include disturbance. In panel (a), a normalized response of zero indicates that there are no differences between the runs. * These are disturbance-related fluxes that are omitted in the 1-tile/not-disturbed model run.

remaining to support a tall dense canopy that obscures the ground surface and recovers quickly.

The relative impacts of subgrid-scale heterogeneity demonstrated herein are robust given our model-on-model approach which cancels out pre-existing biases. This is evident in model runs using alternative pre-1985 fire and harvest scenarios that are bias-corrected to match their respective means from the observed period (Fig. S4a and b). These alternative scenarios have a limited impact on the modeled statistical distributions of aboveground tree biomass (Figs. 5a and S4c). Moreover, because our statistical analysis focused on the period for which disturbance observations are available (1985–2017), and because of the statistical metrics utilized in our model-on-model comparisons (Eq. 12), the differences in $\Delta\bar{X}_{\text{norm}}$ with these alternative scenarios (Fig. S4d) are an order of magnitude smaller than shown in Fig. 6a. Our evaluations provide insights into the impacts of subgrid-scale heterogeneity alone, further reinforcing its importance and the value of representing it within models.

4 Conclusion: implications for representing disturbance and subgrid-scale heterogeneity in LSMs

The dynamic tiling scheme presented in this study could form the basis for a more detailed representation of land use change and resultant subgrid-scale heterogeneity in CLASSIC, the land surface component of the LSM CanESM (Melton et al., 2020; Seiler et al., 2021; Swart et al., 2019). Our tiling scheme has several advantages over other methods. It uses a relatively large number of dynamic tiles as opposed to a small fixed number of tiles, which allows for a more granular representation of vegetation recovery following disturbance (Shevliakova et al., 2009; Yue et al., 2018a; Naudts et al., 2015; Yang et al., 2010; Stocker et al., 2014). It also explicitly simulates C and energy exchanges using tile average properties rather than grid cell average properties, thus fully simulating the impacts of the removal of vegetation by harvest or fire (Bellassen et al., 2010; Haverd et al., 2014; Melton and Arora, 2014). Most importantly, the scheme is dynamic and has no designated size or age class bins; the number of simulated tiles increases as disturbances occur and are then managed by on-demand or pre-emptive joins (Nabel et al., 2020; Shevliakova et al., 2009; Naudts et al., 2015; Bellassen et al., 2010). The tiling routine adapts its size distribution in response to lower disturbance frequencies, more extreme individual disturbance events, and potentially the addition of new PFTs, while remaining computationally efficient. Finally, the tiling scheme can preserve young, recently disturbed tiles, which may improve its representation of early successional differences in GPP, LAI, and cVeg (Bellassen et al., 2010; Zaehle et al., 2006; Nabel et al., 2020). In the context of pan-Canadian or global offline simulations within CLASSIC, this dynamic tiling scheme presents the opportunity for more detailed and efficient representations

of land use and land cover change (LULCC) than can be achieved by simply increasing the spatial resolution of the model, which is limited by model inputs such as meteorological forcing or coupling considerations within CanESM. Future LULCC representations could implement more complex tile harvesting schemes to represent forest management (i.e., thinning, re-planting, clearcut avoidance, or low-intensity harvest) (Puettmann et al., 2015; Pan et al., 2010) or could introduce tiles to account for new LULCC processes and states such as rangelands, pasture, fertilizer use, and irrigation (Shevliakova et al., 2009). Other disturbances, including insect damage, wind damage, and landslides, could likewise be represented using dynamic tiling. Insects in particular are an important disturbance agent in Canada that have more spatially widespread impacts than fire and harvest but greater variation in severity (Kurz et al., 2008; Chen et al., 2000). Non-stand-replacing impacts such as those due to insect defoliation or drought stress can be detected, but their severity or longer-term impacts remain difficult to quantify. Representing these disturbance events requires consistent spatially explicit time series of the forcings, which are not widely available at present (Pongratz et al., 2018; Erb et al., 2017). This would also require careful consideration of the impacts of the disturbance in question. We can infer from our results that low-severity non-stand-replacing disturbances may not require a tiled representation.

Finally, our model-on-model evaluation provides insights into the biases induced in specific variables by the absence of dynamic tiling or particular dynamic tiling setups, which may also apply to other similar tile-based LSMs/discretized schemes (Nabel et al., 2020; Fisher et al., 2018). These results are strengthened by our model-on-model approach, which acts to cancel out pre-existing biases to demonstrate the impacts of subgrid-scale heterogeneity, and discretization error alone (Fig. S4) (Torres-Rojas et al., 2022; Curasi et al., 2023b; Melton et al., 2017; Melton and Arora 2014; Moorcroft et al., 2001). Representing subgrid-scale stand structure leads to differences in land-use emissions if particular size or age classes within the grid cell are preferentially impacted by fire or harvest (Nabel et al., 2020; Shevliakova et al., 2009; Yue et al., 2018b). Our results suggest that representing a relatively small number of heterogeneous tiles may yield undesirable biases when compared to simulations using a larger number of tiles (Figs. 4a–h and 6a) (Yue et al., 2018a; Shevliakova et al., 2009; Stocker et al., 2014; Yang et al., 2010). For a tile-based LSM to represent these subgrid impacts, the simulation needs to be sufficiently complex and judiciously implemented and tested. In the case of CLASSIC, we find that 7–12 tiles optimally balances a detailed representation and computational costs. Using an *rht* of 0.16 and a *tp* of 4 increases computation efficiency with little impact on the level of detail represented. Likewise, subgrid-scale stand structure impacts C fluxes, vegetation C stocks, and energy fluxes (Erb et al., 2017; Luyssaert et al., 2014; Körner, 2006; Dore et al., 2010). These subgrid-scale impacts can be of a similar mag-

nitude to the impacts of disturbance alone, further reinforcing their significance (Fig. 6).

Ultimately, Canadian forest ecosystems are critical components of the global C cycle which are responding to unprecedented climate change. Quantifying historical disturbances and evaluating the impacts of different methods of representing disturbance will improve the representation of the terrestrial C cycle in LSMs. This understanding will also facilitate a comprehensive, process-based assessment of Canada's future terrestrial C cycle and its response to both disturbance events and climate change.

Code and data availability. The Canadian Forest Service land cover and maps of forest disturbance described herein for Canada's forested ecosystems are open access and freely available at https://opendata.nfis.org/mapserver/nfis-change_eng.html (NFIS, 2022). The Stinson et al. (2019) forest management product is available through the Government of Canada's Open Data Portal (<https://open.canada.ca/data/en/dataset/d8fa9a38-c4df-442a-8319-9bbcbdc29060>, Natural Resources Canada, 2019). The current version of CLASSIC is available via the project website: <https://gitlab.com/ccma/classic> (Melton, 2021). The model version, additional software, setup files, and outputs used herein are archived on Zenodo (<https://doi.org/10.5281/zenodo.8302974>, Curasi et al., 2023a).

Supplement. The supplement related to this article is available online at: <https://doi.org/10.5194/gmd-17-2683-2024-supplement>.

Author contributions. SRC, JRM, and ERH conceived the analysis and methodology. SRC conducted the formal analysis, visualization, and software development and wrote the original draft. JRM and ERH obtained funding for and oversaw the work. TH and MAW contributed the National Terrestrial Ecosystem Monitoring System data and contributed to disturbance-forcing development. All authors contributed to writing and editing the manuscript.

Competing interests. The contact author has declared that none of the authors has any competing interests.

Disclaimer. Publisher's note: Copernicus Publications remains neutral with regard to jurisdictional claims made in the text, published maps, institutional affiliations, or any other geographical representation in this paper. While Copernicus Publications makes every effort to include appropriate place names, the final responsibility lies with the authors.

Acknowledgements. We would like to thank Mike Brady (ECCC) for his assistance in processing the disturbance data, Ed Chan for his assistance with the model software and setting up the original model initialization files and meteorological drivers, and Libo Wang

for creating the original land cover products and cross-walking tables. We also thank the anonymous reviewers for their constructive comments.

Financial support. This research has been supported by the Natural Sciences and Engineering Research Council of Canada (NSERC) (grant no. ALLRP 556430-2020).

Review statement. This paper was edited by Sam Rabin and reviewed by two anonymous referees.

References

- Arora, V. K.: Simulating energy and carbon fluxes over winter wheat using coupled land surface and terrestrial ecosystem models, *Agr. Forest Meteorol.*, 118, 21–47, 2003.
- Arora, V. K. and Boer, G. J.: Fire as an interactive component of dynamic vegetation models, *J. Geophys. Res.*, 110, <https://doi.org/10.1029/2005jg000042>, 2005.
- Arora, V. K. and Boer, G. J.: Uncertainties in the 20th century carbon budget associated with land use change, *Glob. Change Biol.*, 16, 3327–3348, 2010.
- Arora, V. K. and Melton, J. R.: Reduction in global area burned and wildfire emissions since 1930s enhances carbon uptake by land, *Nat. Commun.*, 9, 1326, 2018.
- Asaadi, A. and Arora, V. K.: Implementation of nitrogen cycle in the CLASSIC land model, *Biogeosciences*, 18, 669–706, <https://doi.org/10.5194/bg-18-669-2021>, 2021.
- Asaadi, A., Arora, V. K., Melton, J. R., and Bartlett, P.: An improved parameterization of leaf area index (LAI) seasonality in the Canadian Land Surface Scheme (CLASS) and Canadian Terrestrial Ecosystem Model (CTEM) modelling framework, *Biogeosciences*, 15, 6885–6907, <https://doi.org/10.5194/bg-15-6885-2018>, 2018.
- Babst, F., Bouriaud, O., Poulter, B., Trouet, V., Girardin, M. P., and Frank, D. C.: Twentieth century redistribution in climatic drivers of global tree growth, *Sci. Adv.*, 5, eaat4313, <https://doi.org/10.1126/sciadv.aat4313>, 2019.
- Beaudoin, A., Bernier, P. Y., Villemaire, P., Guindon, L., and Guo, X. J.: Tracking forest attributes across Canada between 2001 and 2011 using a k nearest neighbors mapping approach applied to MODIS imagery, *Can. J. Forest Res.*, 48, 85–93, 2018.
- Bellassen, V., Le Maire, G., Dhôte, J. F., Ciais, P., and Viovy, N.: Modelling forest management within a global vegetation model – Part 1: Model structure and general behaviour, *Ecol. Modell.*, 221, 2458–2474, 2010.
- Bond-Lamberty, B. and Gower, S. T.: Decomposition and Fragmentation of Coarse Woody Debris: Re-visiting a Boreal Black Spruce Chronosequence, *Ecosystems*, 11, 831–840, 2008.
- Böttcher, H., Kurz, W. A., and Freibauer, A.: Accounting of forest carbon sinks and sources under a future climate protocol—factoring out past disturbance and management effects on age-class structure, *Environ. Sci. Policy*, 11, 669–686, 2008.
- Bright, R. M., Astrup, R., and Strømman, A. H.: Empirical models of monthly and annual albedo in managed boreal forests of interior Norway, *Climatic Change*, 120, 183–196, 2013.

- Chaste, E., Girardin, M. P., Kaplan, J. O., Portier, J., Bergeron, Y., and Hély, C.: The pyrogeography of eastern boreal Canada from 1901 to 2012 simulated with the LPJ-LMfire model, *Biogeosciences*, 15, 1273–1292, <https://doi.org/10.5194/bg-15-1273-2018>, 2018.
- Chen, J., Chen, W., Liu, J., Cihlar, J., and Gray, S.: Annual carbon balance of Canada's forests during 1895–1996, *Global Biogeochem. Cy.*, 14, 839–849, 2000.
- Chen, J. M., Ju, W., Cihlar, J., Price, D., Liu, J., Chen, W., Pan, J., Black, A., and Barr, A.: Spatial distribution of carbon sources and sinks in Canada's forests, *Tellus B*, 55, 622–641, 2003.
- Curasi, S. R., Melton, J. R., Humphreys, E. R., Hermosilla, T., and Wulder, M. A.: Implementing a dynamic representation of fire and harvest including subgrid-scale heterogeneity in a tile-based land surface model, Zenodo [code and data set], <https://doi.org/10.5281/zenodo.8302974>, 2023a.
- Curasi, S. R., Melton, J. R., Humphreys, E. R., Wang, L., Seiler, C., Cannon, A. J., Chan, E., and Qu, B.: Evaluating the Performance of the Canadian Land Surface Scheme Including Biogeochemical Cycles (CLASSIC) Tailored to the Pan-Canadian Domain, *J. Adv. Model. Earth Sy.*, 15, e2022MS003480, <https://doi.org/10.1029/2022MS003480>, 2023b.
- Czimeczik, C. I., Trumbore, S. E., Carbone, M. S., and Winston, G. C.: Changing sources of soil respiration with time since fire in a boreal forest, *Glob. Change Biol.*, 12, 957–971, 2006.
- D'Orangeville, L., Houle, D., Duchesne, L., Phillips, R. P., Bergeron, Y., and Kneeshaw, D.: Beneficial effects of climate warming on boreal tree growth may be transitory, *Nat. Commun.*, 9, 3213, 2018.
- Dore, S., Kolb, T. E., Montes-Helu, M., Eckert, S. E., Sullivan, B. W., Hungate, B. A., Kaye, J. P., Hart, S. C., Koch, G. W., and Finkral, A.: Carbon and water fluxes from ponderosa pine forests disturbed by wildfire and thinning, *Ecol. Appl.*, 20, 663–683, 2010.
- Earth System Research Laboratory (NOAA/ESRL): Trends in atmospheric carbon dioxide, National Oceanic & Atmospheric Administration, <http://www.esrl.noaa.gov/gmd/ccgg/trends/global.html>, (last access: 11 March 2022).
- ECMWF: ERA5 reanalysis (0.25 degree latitude-longitude grid), ECMWF [data set], <https://www.ecmwf.int/en/forecasts/dataset/ecmwf-reanalysis-v5> (last access: 11 March 2022), 2019.
- Ellner, S. P. and Guckenheimer, J.: *Dynamic Models in Biology*, Princeton University Press, ISBN 9780691125893, 2011.
- Erb, K.-H., Luysaert, S., Meyfroidt, P., Pongratz, J., Don, A., Kloster, S., Kuemmerle, T., Fetzel, T., Fuchs, R., Herold, M., Haberl, H., Jones, C. D., Marín-Spiotta, E., McCallum, I., Robertson, E., Seufert, V., Fritz, S., Valade, A., Wiltshire, A., and Dolman, A. J.: Land management: data availability and process understanding for global change studies, *Glob. Change Biol.*, 23, 512–533, 2017.
- Fisher, R. A., Koven, C. D., Anderegg, W. R. L., Christoffersen, B. O., Dietze, M. C., Farrior, C. E., Holm, J. A., Hurtt, G. C., Knox, R. G., Lawrence, P. J., Lichstein, J. W., Longo, M., Matheny, A. M., Medvigy, D., Muller-Landau, H. C., Powell, T. L., Serbin, S. P., Sato, H., Shuman, J. K., Smith, B., Trugman, A. T., Viskari, T., Verbeeck, H., Weng, E., Xu, C., Xu, X., Zhang, T., and Moorcroft, P. R.: Vegetation demographics in Earth System Models: A review of progress and priorities, *Glob. Change Biol.*, 24, 35–54, 2018.
- Friedlingstein, P., Jones, M. W., O'Sullivan, M., Andrew, R. M., Hauck, J., Peters, G. P., Peters, W., Pongratz, J., Sitch, S., Le Quéré, C., Bakker, D. C. E., Canadell, J. G., Ciais, P., Jackson, R. B., Anthoni, P., Barbero, L., Bastos, A., Bastrikov, V., Becker, M., Bopp, L., Buitenhuis, E., Chandra, N., Chevallier, F., Chini, L. P., Currie, K. I., Feely, R. A., Gehlen, M., Gilfillan, D., Gkritzalis, T., Goll, D. S., Gruber, N., Gutekunst, S., Harris, I., Haverd, V., Houghton, R. A., Hurtt, G., Ilyina, T., Jain, A. K., Joetzer, E., Kaplan, J. O., Kato, E., Klein Goldewijk, K., Korsbakken, J. I., Landschützer, P., Lauvset, S. K., Lefèvre, N., Lenton, A., Lienert, S., Lombardozzi, D., Marland, G., McGuire, P. C., Melton, J. R., Metzl, N., Munro, D. R., Nabel, J. E. M. S., Nakaoka, S.-I., Neill, C., Omar, A. M., Ono, T., Peregón, A., Pierrot, D., Poulter, B., Rehder, G., Resplandy, L., Robertson, E., Rödenbeck, C., Séférian, R., Schwinger, J., Smith, N., Tans, P. P., Tian, H., Tilbrook, B., Tubiello, F. N., van der Werf, G. R., Wiltshire, A. J., and Zaehle, S.: Global Carbon Budget 2019, *Earth Syst. Sci. Data*, 11, 1783–1838, <https://doi.org/10.5194/essd-11-1783-2019>, 2019.
- Friedlingstein, P., Jones, M. W., O'Sullivan, M., Andrew, R. M., Bakker, D. C. E., Hauck, J., Le Quéré, C., Peters, G. P., Peters, W., Pongratz, J., Sitch, S., Canadell, J. G., Ciais, P., Jackson, R. B., Alin, S. R., Anthoni, P., Bates, N. R., Becker, M., Belloin, N., Bopp, L., Chau, T. T. T., Chevallier, F., Chini, L. P., Cronin, M., Currie, K. I., Decharme, B., Djeutchouang, L. M., Dou, X., Evans, W., Feely, R. A., Feng, L., Gasser, T., Gilfillan, D., Gkritzalis, T., Grassi, G., Gregor, L., Gruber, N., Gürses, Ö., Harris, I., Houghton, R. A., Hurtt, G. C., Iida, Y., Ilyina, T., Luijckx, I. T., Jain, A., Jones, S. D., Kato, E., Kennedy, D., Klein Goldewijk, K., Knauer, J., Korsbakken, J. I., Körtzinger, A., Landschützer, P., Lauvset, S. K., Lefèvre, N., Lienert, S., Liu, J., Marland, G., McGuire, P. C., Melton, J. R., Munro, D. R., Nabel, J. E. M. S., Nakaoka, S.-I., Niwa, Y., Ono, T., Pierrot, D., Poulter, B., Rehder, G., Resplandy, L., Robertson, E., Rödenbeck, C., Rosan, T. M., Schwinger, J., Schwingshackl, C., Séférian, R., Sutton, A. J., Sweeney, C., Tanhua, T., Tans, P. P., Tian, H., Tilbrook, B., Tubiello, F., van der Werf, G. R., Vuichard, N., Wada, C., Wanninkhof, R., Watson, A. J., Willis, D., Wiltshire, A. J., Yuan, W., Yue, C., Yue, X., Zaehle, S., and Zeng, J.: Global Carbon Budget 2021, *Earth Syst. Sci. Data*, 14, 1917–2005, <https://doi.org/10.5194/essd-14-1917-2022>, 2022.
- Gelman, A. and Hill, J.: *Data Analysis Using Regression and Multi-level/Hierarchical Models*, Cambridge University Press, 651 pp., 2006.
- Gillis, M. D., Omule, A. Y., and Brierley, T.: Monitoring Canada's forests: The National Forest Inventory, *Forest. Chron.*, 81, 214–221, 2005.
- Girardin, M. P., Bouriaud, O., Hogg, E. H., Kurz, W., Zimmermann, N. E., Metsaranta, J. M., de Jong, R., Frank, D. C., Esper, J., Büntgen, U., Guo, X. J., and Bhatti, J.: No growth stimulation of Canada's boreal forest under half-century of combined warming and CO₂ fertilization, *P. Natl. Acad. Sci. USA*, 113, E8406–E8414, 2016.
- Goetz, S. J., Bunn, A. G., Fiske, G. J., and Houghton, R. A.: Satellite-observed photosynthetic trends across boreal North America associated with climate and fire disturbance, *P. Natl. Acad. Sci. USA*, 102, 13521–13525, 2005.
- Haverd, V., Smith, B., Nieradzki, L. P., and Briggs, P. R.: A stand-alone tree demography and landscape structure module

- for Earth system models: integration with inventory data from temperate and boreal forests, *Biogeosciences*, 11, 4039–4055, <https://doi.org/10.5194/bg-11-4039-2014>, 2014.
- Hayes, D. J., Turner, D. P., Stinson, G., McGuire, A. D., Wei, Y., West, T. O., Heath, L. S., Jong, B., McConkey, B. G., Birdsey, R. A., Kurz, W. A., Jacobson, A. R., Huntzinger, D. N., Pan, Y., Post, W. M., and Cook, R. B.: Reconciling estimates of the contemporary North American carbon balance among terrestrial biosphere models, atmospheric inversions, and a new approach for estimating net ecosystem exchange from inventory-based data, *Glob. Change Biol.*, 18, 1282–1299, 2012.
- Hember, R. A., Kurz, W. A., Metsaranta, J. M., Black, T. A., Guy, R. D., and Coops, N. C.: Accelerating regrowth of temperate-maritime forests due to environmental change, *Glob. Change Biol.*, 18, 2026–2040, 2012.
- Hermosilla, T., Wulder, M. A., White, J. C., Coops, N. C., and Hobart, G. W.: An integrated Landsat time series protocol for change detection and generation of annual gap-free surface reflectance composites, *Remote Sens. Environ.*, 158, 220–234, 2015a.
- Hermosilla, T., Wulder, M. A., White, J. C., Coops, N. C., and Hobart, G. W.: Regional detection, characterization, and attribution of annual forest change from 1984 to 2012 using Landsat-derived time-series metrics, *Remote Sens. Environ.*, 170, 121–132, 2015b.
- Hermosilla, T., Wulder, M. A., White, J. C., Coops, N. C., Hobart, G. W., and Campbell, L. B.: Mass data processing of time series Landsat imagery: pixels to data products for forest monitoring, *Int. J. Digit. Earth*, 9, 1035–1054, 2016.
- Hermosilla, T., Wulder, M. A., White, J. C., Coops, N. C., and Hobart, G. W.: Disturbance-Informed Annual Land Cover Classification Maps of Canada's Forested Ecosystems for a 29-Year Landsat Time Series, *Can. J. Remote Sens.*, 44, 67–87, 2018.
- Hermosilla, T., Wulder, M. A., White, J. C., and Coops, N. C.: Prevalence of multiple forest disturbances and impact on vegetation regrowth from interannual Landsat time series (1985–2015), *Remote Sens. Environ.*, 233, 111403, <https://doi.org/10.1016/j.rse.2019.111403>, 2019.
- Hijmans, R. J., Van Etten, J., Cheng, J., Mattiuzzi, M., Sumner, M., Greenberg, J. A., Lamigueiro, O. P., Bevan, A., Racine, E. B., Shortridge, A., and Hijmans, M. R. J.: Package “raster,” R package, 734, <https://cran.r-project.org/web/packages/raster/index.html> (last access: 11 March 2022), 2015.
- Hirano, T., Suzuki, K., and Hirata, R.: Energy balance and evapotranspiration changes in a larch forest caused by severe disturbance during an early secondary succession, *Agr. Forest Meteorol.*, 232, 457–468, 2017.
- Ju, J. and Masek, J. G.: The vegetation greenness trend in Canada and US Alaska from 1984–2012 Landsat data, *Remote Sens. Environ.*, 176, 1–16, 2016.
- Ju, W. and Chen, J. M.: Simulating the effects of past changes in climate, atmospheric composition, and fire disturbance on soil carbon in Canada's forests and wetlands, *Global Biogeochem. Cy.*, 22, <https://doi.org/10.1029/2007GB002935>, 2008.
- Keenan, T. F. and Williams, C. A.: The Terrestrial Carbon Sink, *Annu. Rev. Env. Resour.*, 43, 219–243, 2018.
- Kim, H.: Global soil wetness project phase 3 atmospheric boundary conditions (Experiment 1), Data Integration and Analysis System (DIAS), Institute of Industrial Science, The University of Tokyo, Tokyo Japan [data set], 2017.
- Körner, C.: Plant CO₂ responses: an issue of definition, time and resource supply, *New Phytol.*, 172, 393–411, 2006.
- Kucharik, C. J., Foley, J. A., Delire, C., Fisher, V. A., Coe, M. T., Lenters, J. D., Young-Molling, C., Ramankutty, N., Norman, J. M., and Gower, S. T.: Testing the performance of a dynamic global ecosystem model: Water balance, carbon balance, and vegetation structure, *Global Biogeochem. Cy.*, 14, 795–825, 2000.
- Kurz, W. A. and Apps, M. J.: Contribution of northern forests to the global C cycle: Canada as a case study, *Water Air Soil Pollut.*, 70, 163–176, 1993.
- Kurz, W. A. and Apps, M. J.: A 70-year retrospective analysis of carbon fluxes in the Canadian forest sector, *Ecol. Appl.*, 9, 526–547, 1999.
- Kurz, W. A., Apps, M. J., Beukema, S. J., and Lekstrum, T.: 20th century carbon budget of Canadian forests, *Tellus B*, 47, 170–177, 1995.
- Kurz, W. A., Beukema, S. J., and Apps, M. J.: Carbon budget implications of the transition from natural to managed disturbance regimes in forest landscapes, *Mitig. Adapt. Strat. Gl.*, 2, 405–421, 1997.
- Kurz, W. A., Stinson, G., Rampley, G. J., Dymond, C. C., and Neilson, E. T.: Risk of natural disturbances makes future contribution of Canada's forests to the global carbon cycle highly uncertain, *P. Natl. Acad. Sci. USA*, 105, 1551–1555, 2008.
- Kurz, W. A., Dymond, C. C., White, T. M., Stinson, G., Shaw, C. H., Rampley, G. J., Smyth, C., Simpson, B. N., Neilson, E. T., Trofymow, J. A., Metsaranta, J., and Apps, M. J.: CBM-CFS3: A model of carbon-dynamics in forestry and land-use change implementing IPCC standards, *Ecol. Modell.*, 220, 480–504, 2009.
- Kuuluvainen, T. and Gauthier, S.: Young and old forest in the boreal: critical stages of ecosystem dynamics and management under global change, *Forest Ecosystems*, 5, 26, <https://doi.org/10.1186/s40663-018-0142-2>, 2018.
- Lange, S.: WFDE5 over land merged with ERA5 over the ocean (W5E5), V1.0, GFZ Data Services, Potsdam, Germany, 2019.
- Lange, S.: ISIMIP3BASD (Version 2.3), Zenodo [data set], <https://doi.org/10.5281/zenodo.3648654>, 2020a.
- Lange, S.: The Inter-Sectoral Impact Model Intercomparison Project Input data set: GSWP3-W5E5, The Inter-Sectoral Impact Model Intercomparison Project [data set], <https://www.isimip.org/gettingstarted/input-data-bias-correction/details/80/> (last access: 11 March 2022), 2020b.
- Latifovic, R., Pouliot, D., and Olthof, I.: Circa 2010 Land Cover of Canada: Local Optimization Methodology and Product Development, *Remote Sens.-Basel*, 9, 1098, <https://doi.org/10.3390/rs9111098>, 2017.
- Le Quéré, C., Andrew, R. M., Friedlingstein, P., Sitch, S., Hauck, J., Pongratz, J., Pickers, P. A., Korsbakken, J. I., Peters, G. P., Canadell, J. G., Arneeth, A., Arora, V. K., Barbero, L., Bastos, A., Bopp, L., Chevallier, F., Chini, L. P., Ciais, P., Doney, S. C., Gkritzalis, T., Goll, D. S., Harris, I., Haverd, V., Hoffman, F. M., Hoppema, M., Houghton, R. A., Hurtt, G., Ilyina, T., Jain, A. K., Johannessen, T., Jones, C. D., Kato, E., Keeling, R. F., Goldewijk, K. K., Landschützer, P., Lefèvre, N., Lienert, S., Liu, Z., Lombardozzi, D., Metzl, N., Munro, D. R., Nabel, J. E. M. S., Nakaoka, S., Neill, C., Olsen, A., Ono, T., Patra, P., Peregón,

- A., Peters, W., Peylin, P., Pfeil, B., Pierrot, D., Poulter, B., Reider, G., Resplandy, L., Robertson, E., Rocher, M., Rödenbeck, C., Schuster, U., Schwinger, J., Séférian, R., Skjelvan, I., Steinhoff, T., Sutton, A., Tans, P. P., Tian, H., Tilbrook, B., Tubiello, F. N., van der Laan-Luijkx, I. T., van der Werf, G. R., Viovy, N., Walker, A. P., Wiltshire, A. J., Wright, R., Zaehle, S., and Zheng, B.: Global Carbon Budget 2018, *Earth Syst. Sci. Data*, 10, 2141–2194, <https://doi.org/10.5194/essd-10-2141-2018>, 2018.
- Lenton, T. M., Held, H., Kriegler, E., Hall, J. W., Lucht, W., Rahmstorf, S., and Schellnhuber, H. J.: Tipping elements in the Earth's climate system, *P. Natl. Acad. Sci. USA*, 105, 1786–1793, 2008.
- Li, R. and Arora, V. K.: Effect of mosaic representation of vegetation in land surface schemes on simulated energy and carbon balances, *Biogeosciences*, 9, 593–605, <https://doi.org/10.5194/bg-9-593-2012>, 2012.
- Liu, H.: Changes in the surface energy budget after fire in boreal ecosystems of interior Alaska: An annual perspective, *J. Geophys. Res.*, 110, <https://doi.org/10.1029/2004jd005158>, 2005.
- Luyssaert, S., Jammot, M., Stoy, P. C., Estel, S., Pongratz, J., Ceschia, E., Churkina, G., Don, A., Erb, K., Ferlicoq, M., Giesen, B., Grünwald, T., Houghton, R. A., Klumpp, K., Knohl, A., Kolb, T., Kuemmerle, T., Laurila, T., Lohila, A., Loustau, D., McGrath, M. J., Meyfroidt, P., Moors, E. J., Naudts, K., Novick, K., Otto, J., Pilegaard, K., Pio, C. A., Rambal, S., Rebmann, C., Ryder, J., Suyker, A. E., Varlagin, A., Wattenbach, M., and Dolman, A. J.: Land management and land-cover change have impacts of similar magnitude on surface temperature, *Nat. Clim. Change*, 4, 389–393, 2014.
- Ma, Z., Peng, C., Zhu, Q., Chen, H., Yu, G., Li, W., Zhou, X., Wang, W., and Zhang, W.: Regional drought-induced reduction in the biomass carbon sink of Canada's boreal forests, *P. Natl. Acad. Sci. USA*, 109, 2423–2427, 2012.
- MacKay, M. D., Meyer, G., and Melton, J. R.: On the Discretization of Richards Equation in Canadian Land Surface Models, *Atmos. Ocean*, 6, 1–11, 2022.
- MacKenzie, W. H. and Meidinger, D. V.: The Biogeoclimatic Ecosystem Classification Approach: an ecological framework for vegetation classification, *Phytocoenologia*, 48, 203–213, 2018.
- Maltman, J. C., Hermosilla, T., Wulder, M. A., Coops, N. C., and White, J. C.: Estimating and mapping forest age across Canada's forested ecosystems, *Remote Sens. Environ.*, 290, 113529, <https://doi.org/10.1016/j.rse.2023.113529>, 2023.
- Maness, H., Kushner, P. J., and Fung, I.: Summertime climate response to mountain pine beetle disturbance in British Columbia, *Nat. Geosci.*, 6, 65–70, 2012.
- Marchand, W., Girardin, M. P., Gauthier, S., Hartmann, H., Bouriaud, O., Babst, F., and Bergeron, Y.: Untangling methodological and scale considerations in growth and productivity trend estimates of Canada's forests, *Environ. Res. Lett.*, 13, 093001, <https://doi.org/10.1088/1748-9326/aad82a>, 2018.
- Melton, J.: CLASSIC, *GitLab [code]*, <https://gitlab.com/ccma/classic> (last access: 11 March 2022), 2021.
- Melton, J. R. and Arora, V. K.: Sub-grid scale representation of vegetation in global land surface schemes: implications for estimation of the terrestrial carbon sink, *Biogeosciences*, 11, 1021–1036, <https://doi.org/10.5194/bg-11-1021-2014>, 2014.
- Melton, J. R. and Arora, V. K.: Competition between plant functional types in the Canadian Terrestrial Ecosystem Model (CTEM) v. 2.0, *Geosci. Model Dev.*, 9, 323–361, <https://doi.org/10.5194/gmd-9-323-2016>, 2016.
- Melton, J. R., Sospedra-Alfonso, R., and McCusker, K. E.: Tiling soil textures for terrestrial ecosystem modelling via clustering analysis: a case study with CLASS-CTEM (version 2.1), *Geosci. Model Dev.*, 10, 2761–2783, <https://doi.org/10.5194/gmd-10-2761-2017>, 2017.
- Melton, J. R., Arora, V. K., Wisernig-Cojoc, E., Seiler, C., Fortier, M., Chan, E., and Teckentrup, L.: CLASSIC v1.0: the open-source community successor to the Canadian Land Surface Scheme (CLASS) and the Canadian Terrestrial Ecosystem Model (CTEM) – Part 1: Model framework and site-level performance, *Geosci. Model Dev.*, 13, 2825–2850, <https://doi.org/10.5194/gmd-13-2825-2020>, 2020.
- Meyer, G., Humphreys, E. R., Melton, J. R., Cannon, A. J., and Lafleur, P. M.: Simulating shrubs and their energy and carbon dioxide fluxes in Canada's Low Arctic with the Canadian Land Surface Scheme Including Biogeochemical Cycles (CLASSIC), *Biogeosciences*, 18, 3263–3283, <https://doi.org/10.5194/bg-18-3263-2021>, 2021.
- Moorcroft, P. R., Hurtt, G. C., and Pacala, S. W.: A Method For Scaling Vegetation Dynamics: The Ecosystem Demography Model (Ed), *Ecol. Monogr.*, 71, 557–586, 2001.
- Nabel, J. E. M. S., Naudts, K., and Pongratz, J.: Accounting for forest age in the tile-based dynamic global vegetation model JSBACH4 (4.20p7; git feature/forests) – a land surface model for the ICON-ESM, *Geosci. Model Dev.*, 13, 185–200, <https://doi.org/10.5194/gmd-13-185-2020>, 2020.
- Natural Resources Canada: Map of Forest Management in Canada, Natural Resources Canada [data set], <https://open.canada.ca/data/en/dataset/d8fa9a38-c4df-442a-8319-9bbcbdc29060> (last access: 11 March 2022), 2019.
- Naudts, K., Ryder, J., McGrath, M. J., Otto, J., Chen, Y., Valade, A., Bellasen, V., Berhongaray, G., Bönsch, G., Campioli, M., Ghattas, J., De Groote, T., Haverd, V., Kattge, J., MacBean, N., Maignan, F., Merilä, P., Penuelas, J., Peylin, P., Pinty, B., Pretzsch, H., Schulze, E. D., Solyga, D., Vuichard, N., Yan, Y., and Luyssaert, S.: A vertically discretised canopy description for ORCHIDEE (SVN r2290) and the modifications to the energy, water and carbon fluxes, *Geosci. Model Dev.*, 8, 2035–2065, <https://doi.org/10.5194/gmd-8-2035-2015>, 2015.
- NFIS: National Terrestrial Ecosystem Monitoring System for Canada, NFIS [data set], https://opendata.nfis.org/mapserver/nfis-change_eng.html, last access: 11 March 2022.
- Nocedal, J., and Wright, S. J.: Numerical Optimization, edited by: Mikshch, T. V., Resnick, S. I., and Robinson, S. M., Springer Science+Business Media, 2006.
- Pan, Y., Chen, J. M., Birdsey, R., McCullough, K., He, L., and Deng, F.: Age structure and disturbance legacy of North American forests, *Biogeosciences*, 8, 715–732, <https://doi.org/10.5194/bg-8-715-2011>, 2011.
- Pan, Y., Birdsey, R. A., Phillips, O. L., and Jackson, R. B.: The Structure, Distribution, and Biomass of the World's Forests, *Annu. Rev. Ecol. Evol. S.*, 44, 593–622, 2013.
- Peng, Y., Arora, V. K., Kurz, W. A., Hember, R. A., Hawkins, B. J., Fyfe, J. C., and Werner, A. T.: Climate and atmospheric drivers of historical terrestrial carbon uptake in the province of British Columbia, Canada, *Biogeosciences*, 11, 635–649, <https://doi.org/10.5194/bg-11-635-2014>, 2014.

- Pongratz, J., Dolman, H., Don, A., Erb, K.-H., Fuchs, R., Herold, M., Jones, C., Kuemmerle, T., Luyssaert, S., Meyfroidt, P., and Naudts, K.: Models meet data: Challenges and opportunities in implementing land management in Earth system models, *Glob. Change Biol.*, 24, 1470–1487, 2018.
- Potapov, P., Hansen, M. C., Stehman, S. V., Loveland, T. R., and Pittman, K.: Combining MODIS and Landsat imagery to estimate and map boreal forest cover loss, *Remote Sens. Environ.*, 112, 3708–3719, 2008.
- Puettmann, K. J., Wilson, S. M., Baker, S. C., Donoso, P. J., Drössler, L., Amente, G., Harvey, B. D., Knoke, T., Lu, Y., Nocentini, S., Putz, F. E., Yoshida, T., and Bauhus, J.: Silvicultural alternatives to conventional even-aged forest management - what limits global adoption?, *Forest Ecosystems*, 2, 1–16, 2015.
- R Core Team: R: A language and environment for statistical computing, The R Foundation for Statistical Computing, c/o Institute for Statistics and Mathematics, Wirtschaftsuniversität Wien, Welthandelsplatz 1, 1020 Vienna, Austria, 2013.
- Reich, P. B., Sendall, K. M., Stefanski, A., Rich, R. L., Hobbie, S. E., and Montgomery, R. A.: Effects of climate warming on photosynthesis in boreal tree species depend on soil moisture, *Nature*, 562, 263–267, 2018.
- Salkfield, T., Walton, A., and Mackenzie, W.: Biogeoclimatic Ecosystem Classification Map, Ministry of Forests, Lands, Natural Resource Operations and Rural Development, <https://catalogue.data.gov.bc.ca/dataset/bec-map> (last access: 7 August 2020), 2016.
- Seiler, C., Melton, J. R., Arora, V. K., and Wang, L.: CLASSIC v1.0: the open-source community successor to the Canadian Land Surface Scheme (CLASS) and the Canadian Terrestrial Ecosystem Model (CTEM) – Part 2: Global benchmarking, *Geosci. Model Dev.*, 14, 2371–2417, <https://doi.org/10.5194/gmd-14-2371-2021>, 2021.
- Shangguan, W., Hengl, T., Mendes de Jesus, J., Yuan, H., and Dai, Y.: Mapping the global depth to bedrock for land surface modeling, *J. Adv. Model. Earth Sy.*, 9, 65–88, 2017.
- Shevliakova, E., Pacala, S. W., Malyshev, S., Hurtt, G. C., Milly, P. C. D., Caspersen, J. P., Sentman, L. T., Fisk, J. P., Wirth, C., and Crevoisier, C.: Carbon cycling under 300 years of land use change: Importance of the secondary vegetation sink, *Global Biogeochem. Cy.*, 23, <https://doi.org/10.1029/2007gb003176>, 2009.
- Shrestha, B. M. and Chen, H. Y. H.: Effects of stand age, wild-fire and clearcut harvesting on forest floor in boreal mixedwood forests, *Plant Soil*, 336, 267–277, 2010.
- Shrestha, R. K., Arora, V. K., and Melton, J. R.: The sensitivity of simulated competition between different plant functional types to subgrid-scale representation of vegetation in a land surface model, *J. Geophys. Res.-Biogeo.*, 121, 809–828, 2016.
- Skakun, R., Whitman, E., Little, J. M., and Parisien, M.-A.: Area burned adjustments to historical wildland fires in Canada, *Environ. Res. Lett.*, 16, 064014, <https://doi.org/10.1088/1748-9326/abfb2c>, 2021.
- Stinson, G., Kurz, W. A., Smyth, C. E., Neilson, E. T., Dymond, C. C., Metsaranta, J. M., Boisvenue, C., Rampley, G. J., Li, Q., White, T. M., and Blain, D.: An inventory-based analysis of Canada's managed forest carbon dynamics, 1990 to 2008, *Glob. Change Biol.*, 17, 2227–2244, 2011.
- Stinson, G., Thandi, G., Aitkin, D., Bailey, C., Boyd, J., Colley, M., Fraser, C., Gelhorn, L., Groenewegen, K., Hogg, A., Kapron, J., Leboeuf, A., Makar, M., Montigny, M., Pittman, B., Price, K., Salkeld, T., Smith, L., Viveiros, A., and Wilson, D.: A new approach for mapping forest management areas in Canada, *Forest. Chron.*, 95, 101–112, 2019.
- Stocker, B. D., Spahni, R., and Joos, F.: DYPTOP: a cost-efficient TOPMODEL implementation to simulate sub-grid spatio-temporal dynamics of global wetlands and peatlands, *Geosci. Model Dev.*, 7, 3089–3110, <https://doi.org/10.5194/gmd-7-3089-2014>, 2014.
- Sulla-Menashe, D., Woodcock, C. E., and Friedl, M. A.: Canadian boreal forest greening and browning trends: an analysis of biogeographic patterns and the relative roles of disturbance versus climate drivers, *Environ. Res. Lett.*, 13, 014007, <https://doi.org/10.1088/1748-9326/aa9b88>, 2018.
- Swart, N. C., Cole, J. N. S., Kharin, V. V., Lazare, M., Scinocca, J. F., Gillett, N. P., Anstey, J., Arora, V., Christian, J. R., Hanna, S., Jiao, Y., Lee, W. G., Majaess, F., Saenko, O. A., Seiler, C., Seinen, C., Shao, A., Sigmund, M., Solheim, L., von Salzen, K., Yang, D., and Winter, B.: The Canadian Earth System Model version 5 (CanESM5.0.3), *Geosci. Model Dev.*, 12, 4823–4873, <https://doi.org/10.5194/gmd-12-4823-2019>, 2019.
- Torres-Rojas, L., Vergopolan, N., Herman, J. D. and Chaney, N. W.: Towards an Optimal Representation of Sub-Grid Heterogeneity in Land Surface Models, *Water Resour. Res.*, 58, e2022WR032233, <https://doi.org/10.1029/2022WR032233>, 2022..
- Van Wagner, C. E.: The historical pattern of annual burned area in Canada, *Forest. Chron.*, 64, 182–185, 1988.
- Verseghy, D.: CLASS—The Canadian land surface scheme (v.3.6.2), Climate Research Division, Science and Technology Branch, Environment Canada, Victoria BC, Canada, 35, 2017.
- Verseghy, D. L.: The Canadian land surface scheme (CLASS): Its history and future, *Atmos. Ocean*, 38, 1–13, 2000.
- Verseghy, D. L.: Class-A Canadian land surface scheme for GCMS. I. Soil model, *Int. J. Climatol.*, 11, 111–133, 2007.
- Verseghy, D. L., McFarlane, N. A., and Lazare, M.: Class—A Canadian land surface scheme for GCMS. II. Vegetation model and coupled runs, *Int. J. Climatol.*, 13, 347–370, 1993.
- Wang, L., Arora, V. K., Bartlett, P., Chan, E., and Curasi, S. R.: Mapping of ESA's Climate Change Initiative land cover data to plant functional types for use in the CLASSIC land model, *Biogeosciences*, 20, 2265–2282, <https://doi.org/10.5194/bg-20-2265-2023>, 2023.
- Weber, M. G. and Flannigan, M. D.: Canadian boreal forest ecosystem structure and function in a changing climate: impact on fire regimes, *Environ. Rev.*, 5, 145–166, 1997.
- White, J. C., Wulder, M. A., Hermosilla, T., Coops, N. C., and Hobart, G. W.: A nationwide annual characterization of 25 years of forest disturbance and recovery for Canada using Landsat time series, *Remote Sens. Environ.*, 194, 303–321, 2017.
- World Resources Institute: Canada's Forests at a Crossroads: An Assessment in the Year 2000: a Global Forest Watch Canada Report, World Resources Institute, Washington DC, USA, 114 pp., 2000.
- Wulder, M. A., Hermosilla, T., White, J. C., and Coops, N. C.: Biomass status and dynamics over Canada's forests: Disentangling disturbed area from associated aboveground

- biomass consequences, *Environ. Res. Lett.*, 15, 094093, <https://doi.org/10.1088/1748-9326/ab8b11>, 2020.
- Yang, X., Richardson, T. K., and Jain, A. K.: Contributions of secondary forest and nitrogen dynamics to terrestrial carbon uptake, *Biogeosciences*, 7, 3041–3050, <https://doi.org/10.5194/bg-7-3041-2010>, 2010.
- Yue, C., Ciais, P., Luysaert, S., Li, W., McGrath, M. J., Chang, J., and Peng, S.: Representing anthropogenic gross land use change, wood harvest, and forest age dynamics in a global vegetation model ORCHIDEE-MICT v8.4.2, *Geosci. Model Dev.*, 11, 409–428, <https://doi.org/10.5194/gmd-11-409-2018>, 2018a.
- Yue, C., Ciais, P., and Li, W.: Smaller global and regional carbon emissions from gross land use change when considering sub-grid secondary land cohorts in a global dynamic vegetation model, *Biogeosciences*, 15, 1185–1201, <https://doi.org/10.5194/bg-15-1185-2018>, 2018b.
- Zaehle, S., Sitch, S., Prentice, I. C., Liski, J., Cramer, W., Erhard, M., Hickler, T., and Smith, B.: The importance of age-related decline in forest NPP for modeling regional carbon balances, *Ecol. Appl.*, 16, 1555–1574, 2006.